Review of Predictions of Hard Probes in p+Pb Collisions at $\sqrt{s_{NN}} = 5.02$ and 8.16 TeV and Comparison With Data

R. Vogt

Lawrence Livermore National Laboratory, Livermore, CA 94551, USA
Physics Department, University of California, Davis, CA 95616, USA

Int. J. Mod. Phys. E 22 (2013) 1330007 [arXiv:1301.3395 [hep-ph]],
Int. J. Mod. Phys. E 25 (2016) 1630005 [arXiv:1605.09479 [hep-ph]]
Nucl. Phys. A 972 (2018) 18 [arXiv:1707.09973 [hep-ph]]

Contributions to calculations in this talk from: F. Arleo *et al.* (J/ψ, Υ, Drell-Yan), G. Barnafoldi *et al.* (HIJING++), D. d'Enterria (top quarks), K. J. Eskola (EPPS16, dijets), E. G. Ferreiro (J/ψ, ψ'), J.-P. Lansberg *et al.* (J/ψ, Υ, heavy flavor), I. Vitev *et al.* (heavy flavor), RV (J/ψ, Υ), B.-W. Zhang *et al* (gauge bosons)

Figure 1: This work was performed under the auspices of the U.S. Department of Energy by Lawrence Livermore National Laboratory under Contract DE-AC52-07NA27344 and supported by the U.S. Department of Energy, Office of Science, Office of Nuclear Physics (Nuclear Theory) under contract number DE-SC-0004014.

Why p+Pb?

- **System is intermediate to 'vacuum of $p+p$ collisions and hot quark-gluon plasma of heavy-ion collision such as Pb+Pb**
- **Comparison to $p+p$ determines level of cold nuclear matter effects, modifications due to the nuclear medium without QGP**
- **Comparisons to Pb+Pb differentiates between cold and hot nuclear matter effects**
- **It's not that straightforward: high multiplicity p+Pb (and even $p+p$) events share some characteristics with heavy-ion collisions**
- **In this talk, the focus is on results from minimum bias collisions with low multiplicities**

Why Hard Probes?

- **Hard probes are produced at early times**
- **They carry information on the state of the system**
- **Some (hard photons, Drell-Yan, gauge bosons) will travel through the system (cold or hot) without further interaction**

Outline

- **Quarkonium and Open Heavy Flavor + Drell-Yan**
- **Nuclear Parton Densities + Updates Since LHC Turn On**
- **Dijets: High Q^2 Probe of Nuclear Gluon Density**
- **Gauge Bosons: Probing Valence and Sea Distributions in Nuclei**

Quarkonium and Open Heavy Flavor

- J/ψ
  - **Collinear Factorization**
  - **CGC - Saturation**
- ψ**(2S): Comovers**
- Υ
- B **mesons**
- **Drell-Yan**

Quarkonium

Quarkonium production is still not settled in p+p collisions, that uncertainty makes interpretation of $p + A$ and $A + A$ less straightforward

Some calculations here are based on the Color Evaporation Model (CEM), some on NRQCD, and others are simply parameterizations of the data

Initial state of system described either through collinear factorization or color glass condensate

- **Collinear factorization involves evolution in Q^2, moderate x, according to DGLAP equations**
- **Color-glass condensate treats system as coherent gluon field, effects in nuclei enhanced by $A^{1/3}$ but effective only at low x below saturation scale $Q^2_{\rm sat}$**

Final-State Energy Loss (Arleo and Peigne)

Arleo and Peigne fit a parameter depending on energy loss and path length to fixed-target data that also depends on L_A to E866 data and uses the same parameter for other energies

$$\frac{1}{A}\frac{d\sigma_{pA}(x_F)}{dx_F} = \int_0^{E_p-E} d\epsilon P(\epsilon)\frac{d\sigma_{pp}(x_F+\delta x_F(\epsilon))}{dx_F}$$

There is no production model, only a parameterization of the pp cross section in p_T and x_F or rapidity y

$$\frac{d\sigma_{pp}}{dp_T dx} = \frac{(1-x)^n}{x}\left(\frac{p_0^2}{(p_0^2+p_T^2)}\right)^m$$

Parameters n and m are fit to pp data, $n \sim 5$ at $\sqrt{s} = 38.8$ GeV, 34 at 2.76 TeV as x_F distribution becomes narrower

Including shadowing as well as energy loss modifies the energy loss parameter, no significant difference in shape of fit at fixed-target energy but significant difference at higher $\sqrt{s}$ – results here shown with only energy loss

Backward x_F/y effect is large for this scenario – at some energy dependent value the shift overtakes the x value in the projectile and the parameterization is invalid

Initial-State Shadowing: RV (5.02 and 8.16 TeV)

We use charm mass and scale fit to total charm data to calculate quarkonium in the color evaporation model (CEM) at NLO
eex

$m = 1.27 \pm 0.09$ **GeV,** $\mu_F/m = 2.10^{+2.55}_{-0.85}$**, and** $\mu_R/m = 1.60^{+0.11}_{-0.12}$

$$\sigma_C^{\rm CEM}(s) = F_C \sum_{i,j} \int_{4m^2}^{4m_H^2} ds \int dx_1\, dx_2\ f_i^p(x_1,\mu_F^2)\ f_j^p(x_2,\mu_F^2)\ \hat{\sigma}_{ij}(\hat{s},\mu_F^2,\mu_R^2)\ ,$$

The EPS09 NLO sets are employed; all sets are used and the uncertainties on the shadowing obtained by adding in quadrature

Initial-State Modifications: Lansberg and Shao (8.16 TeV)

Data-driven approach: parameterization of the $2 \to 2$ gg production channel, parameters are fit to $p+p$ data for quarkonium and heavy flavor production

Results are calculated for EPS09 NLO, EPS09 LO, and nCTEQ15

$$\frac{d\sigma(p+p \to \mathcal{H}+X)}{d\Phi_2} = \frac{1}{2s}\int dx_1 dx_2 x_1 f_p(x_1) x_2 f_p(x_2) \overline{|\mathcal{A}(k_1 k_2 \to \mathcal{H}+k_3)|^2} \ .$$

$$\begin{aligned}\overline{|\mathcal{A}(k_1 k_2 \to \mathcal{H}+k_3)|^2} \ &= \ \frac{\lambda^2 \kappa \, x_1 x_2 s}{M_{\mathcal{H}}^2} \exp\left[-\kappa \min(p_T^2, \langle p_T \rangle^2)/M_{\mathcal{H}}^2)\right] \\ &\times \ \left(1+\theta(p_T^2 - \langle p_T^2 \rangle^2)\frac{\kappa}{n}\frac{p_T^2 - \langle p_T \rangle^2}{M_{\mathcal{H}}^2}\right)^{-n} \ ,\end{aligned}$$

Lansberg and collaborators are using this approach to try and reduce the uncertainties due to shadowing

Initial-State Modifications: Lansberg *et al.* (5.02 TeV)

Leading order color singlet model (CSM) calculates production with EPS09 LO

Differences arise between LO CEM and LO CSM from several circumstances: CEM at LO means $p_T \equiv 0$ while CSM is integrated over p_T; different choices for mass and scale parameters means that even when both use EPS09 LO the results will not be identical due to these values

The 5.02 TeV results show only the two EPS09 LO sets giving the maximum and minimum of gluon shadowing, not uncertainty on all sets taken together

Differences in $R_{p\mathrm{Pb}}$ between EPS09 NLO (CEM) and EPS09 LO (CSM) not due to model or LO vs. NLO

Main source of difference is low x behavior of the proton PDFs:
EPS09 LO + CTEQ61LO flat as $x \to 0$;
EPS09 NLO + CTEQ6M, increasing at low x

Color Glass Condensate with CEM: Ducloué *et al* (8.16 TeV)

CEM cross section

$$\frac{d\sigma_{J/\psi}}{d^2p_T dy} = F_{J/\psi}\int_{4m_c^2}^{4m_D^2} dM^2 \frac{d\sigma_{c\bar{c}}}{d^2p_T dy dM^2}$$

Applicable only in the forward region, where x is small

$$\frac{d\sigma_{c\bar{c}}}{d^2p_T d^2q_T dy_p dy_q} = \frac{\alpha_s^2 N_c}{8\pi^2 d_A}\frac{1}{(2\pi)^2}\int \frac{d^2k_T}{(2\pi)^2}\frac{\Xi_{\rm coll}(p_T+q_T,k_T)}{(p_T+q_T)^2}\phi^{q\bar{q},g}_{y_2=\ln\frac{1}{x_2}}(p_T+q_T,k_T)x_1 g(x_1,Q^2)\ .$$

Here $d_A = N_c^2 - 1$, $x_{1,2} = (\sqrt{p_T^2+M^2})/\sqrt{s}\exp(\pm y)$, $\Xi_{\rm coll}$ is a hard matrix element and

$$\phi_Y^{q\bar{q},g}(l_T,k_T) = \int d^2b_T \frac{N_c l_T^2}{4\alpha_s} S(k_T)S(l_T-k_T)$$

The dipole amplitudes in $S(k_T)$ and $S(l_t-k_T)$ are evaluated at x_2

Color Glass Condensate with CEM: Fuji *et al.* (5.02 TeV)

CGC calculations by Fujii *et al.* are made only in the forward direction where x_2 (in Pb nucleus) is small

Uncertainty comes from varying the saturation scale, $Q^2_{0\mathrm{sat},A} \sim (4-6)Q^2_{0\mathrm{sat},p}$ and the quark masses, $1.2 < m_c < 1.5$ GeV and $4.5 < m_b < 4.8$ GeV

Found large suppression at forward rapidities, much larger than later calculations by other groups

Color Glass Condensate with NRQCD: Ma *et al*

NRQCD separates cross sections by color and spin, $\kappa = {}^{2S+1}L_J^{[c]}$ and $c = 1$ or 8 for color singlet and color octet respectively, nonperturbative long distance matrix elements (LDMEs) are fit to data while short distance cross sections are perturbatively calculated,

$$d\sigma_{pA}^{H} = \sum_{\kappa} d\hat{\sigma}_{pA}^{\kappa} \langle \mathcal{O}_{\kappa}^{H} \rangle$$

$$\text{CS}: \quad \frac{d\hat{\sigma}_{pA}^{\kappa}}{d^2\boldsymbol{p}_T dy} = \frac{\alpha_s(\pi \overline{R}_A^2)}{(2\pi)^9 (N_c^2 - 1)} \int_{\boldsymbol{k}_{1T}, \boldsymbol{k}_T, \boldsymbol{k}'_T} \frac{\varphi_{p,y_p}(\boldsymbol{k}_{1T})}{k_{1T}^2} \mathcal{N}_Y(\boldsymbol{k}_T) \mathcal{N}_Y(\boldsymbol{k}'_T) \mathcal{N}_Y(\boldsymbol{p}_T - \boldsymbol{k}_{1T} - \boldsymbol{k}_T - \boldsymbol{k}'_T)\, \mathcal{G}_1^{\kappa}$$

$$\text{CO}: \quad \frac{d\hat{\sigma}_{pA}^{\kappa}}{d^2\boldsymbol{p}_T dy} = \frac{\alpha_s(\pi \overline{R}_A^2)}{(2\pi)^7 (N_c^2 - 1)} \int_{\boldsymbol{k}_{1T}, \boldsymbol{k}_T} \frac{\varphi_{p,y_p}(\boldsymbol{k}_{1T})}{k_{1T}^2} \mathcal{N}_Y(\boldsymbol{k}_T) \mathcal{N}_Y(\boldsymbol{p}_T - \boldsymbol{k}_{1T} - \boldsymbol{k}_T)\, \Gamma_8^{\kappa}$$

The unintegrated gluon distributions are denoted by φ while $\mathcal{N}$ & $\widetilde{\mathcal{N}}^A$ are the momentum-space dipole forward scattering amplitudes in the fundamental & adjoint representations and the effective transverse areas of the dilute proton and dense nucleus are denoted $\pi \overline{R}_p^2$ & $\pi \overline{R}_A^2$ respectively

Uncertainties arise from those of the LDMEs and are calculated separately for each singlet and octet state

$R_{p\mathrm{Pb}}(y)$ for J/ψ and Υ (5.02 TeV)

NLO shadowing does not describe curvature of data, LO band is larger due to greater uncertainty of EPS09 LO (only min/max used in Lansberg calculation)

Energy loss alone does well for J/ψ $R_{p\mathrm{Pb}}$ but stronger curvature for R_{FB}, unclear for Υ

CGC + CEM (Fujii) below data, CGC + NRQCD (not shown) may agree better

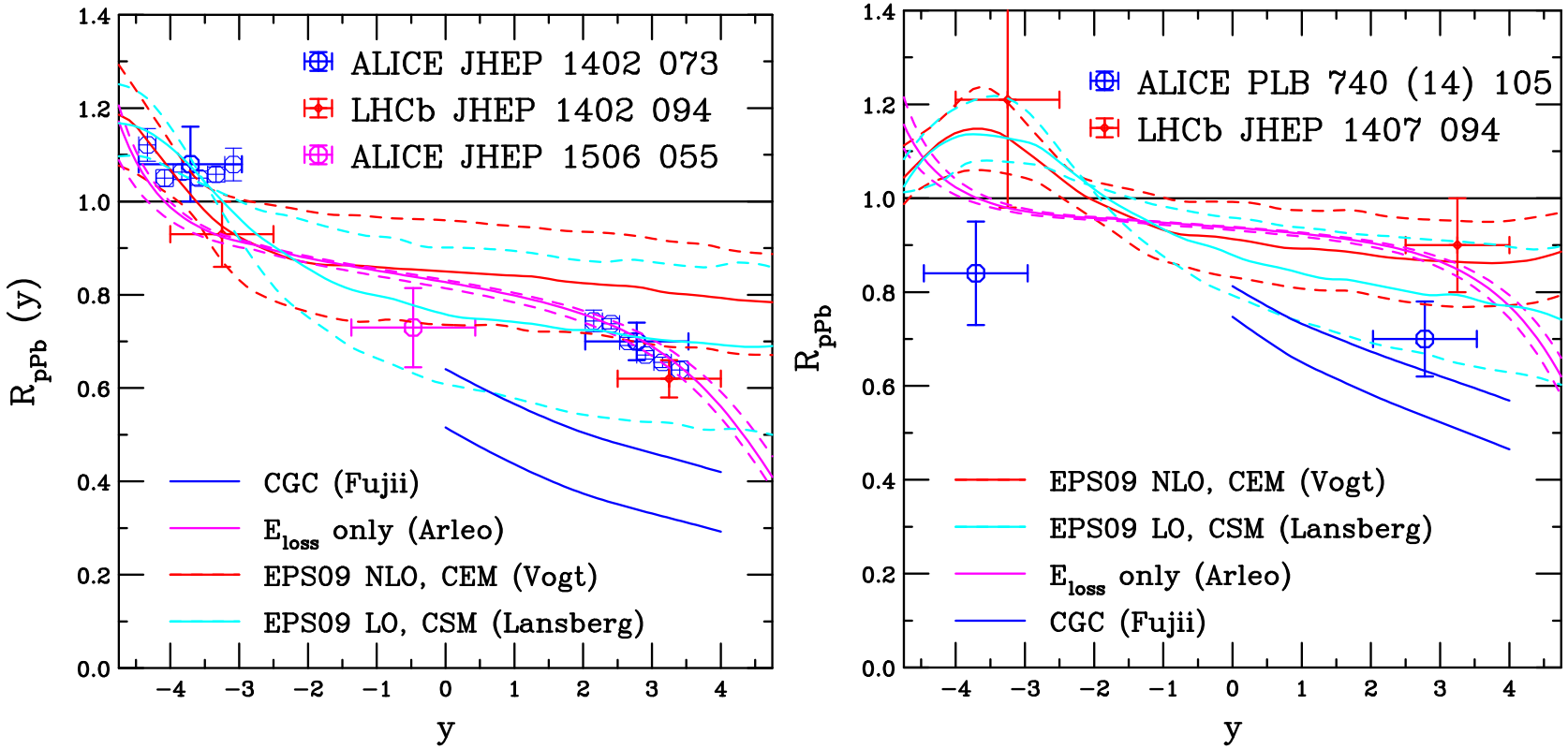

Figure 2: **(Left) The $R_{p\mathrm{Pb}}$ ratio for J/ψ as a function of y. The dashed red histogram shows the EPS09 NLO CEM uncertainties. The EPS09 LO CSM calculation by Lansberg *et al.* is shown in cyan. The energy loss calculation of Arleo and Peigne is shown in magenta. The upper and lower limits of the CGC calculation by Fujii *et al* are in blue at forward rapidity. (Right) The $R_{p\mathrm{Pb}}$ ratio for Υ as a function of y. The dashed red histogram shows the EPS09 NLO CEM uncertainties. The EPS09 LO CSM calculation by Lansberg *et al.* is shown in cyan. The energy loss calculation of Arleo and Peigne is shown in magenta. The upper and lower limits of the CGC calculation by Fujii *et al* are in blue at forward rapidity.**

$R_{p\mathrm{Pb}}(y)$ for J/ψ: 8.16 TeV

Backward rapidity p_T dependence shows antishadowing while, at low p_T, $R_{p\mathrm{Pb}}$ is reduced

Collinear factorization calculations, left and middle, agree with data but CGC calculations show stronger curvature at low p_T, in better agreement with trends

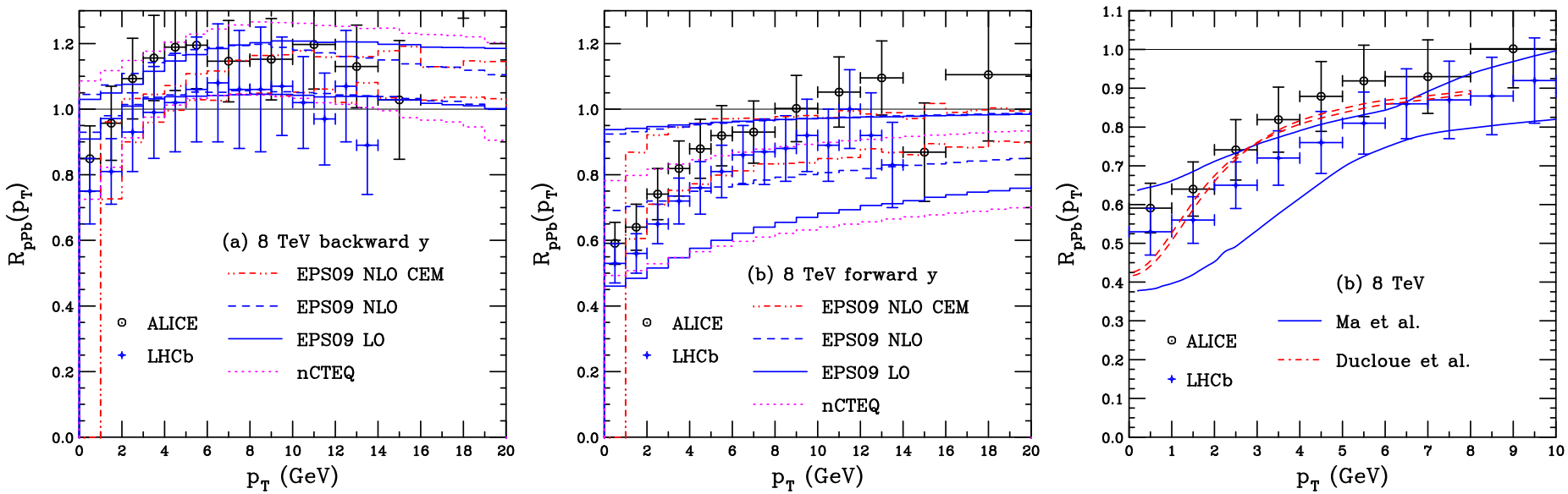

Figure 3: **The ratio $R_{p\mathrm{Pb}}$ for J/ψ as a function of transverse momentum at 8 TeV. (Left and Middle) The EPS09 NLO results of RV (dot-dot-dash-dashed red curve) and Lansberg and Shao (solid cyan) are shown with their results for EPS09 LO (solid blue histogram) and nCTEQ (dotted magenta histogram) at backward (left) and forward (middle) rapidity. (Right) Results at forward rapidity by Doucloué *et al.* (red dashed curves) and Ma *et al.* in the CGC approach are shown. The ALICE data (JHEP 1807 160) at backward and forward rapidity are shown in black while the LHCb data (PLB 774 (2017) 159) are in blue.**

$R_{p\mathrm{Pb}}(p_T)$ for J/ψ: 5 vs. 8 TeV

Data available to higher p_T at 8 TeV

(Left) Backward rapidity shows largest difference at low p_T where both data and calculations show larger reduction at 8 TeV relative to 5 TeV

(Right) Forward rapidity results, both calculations and data, are effectively independent of energy

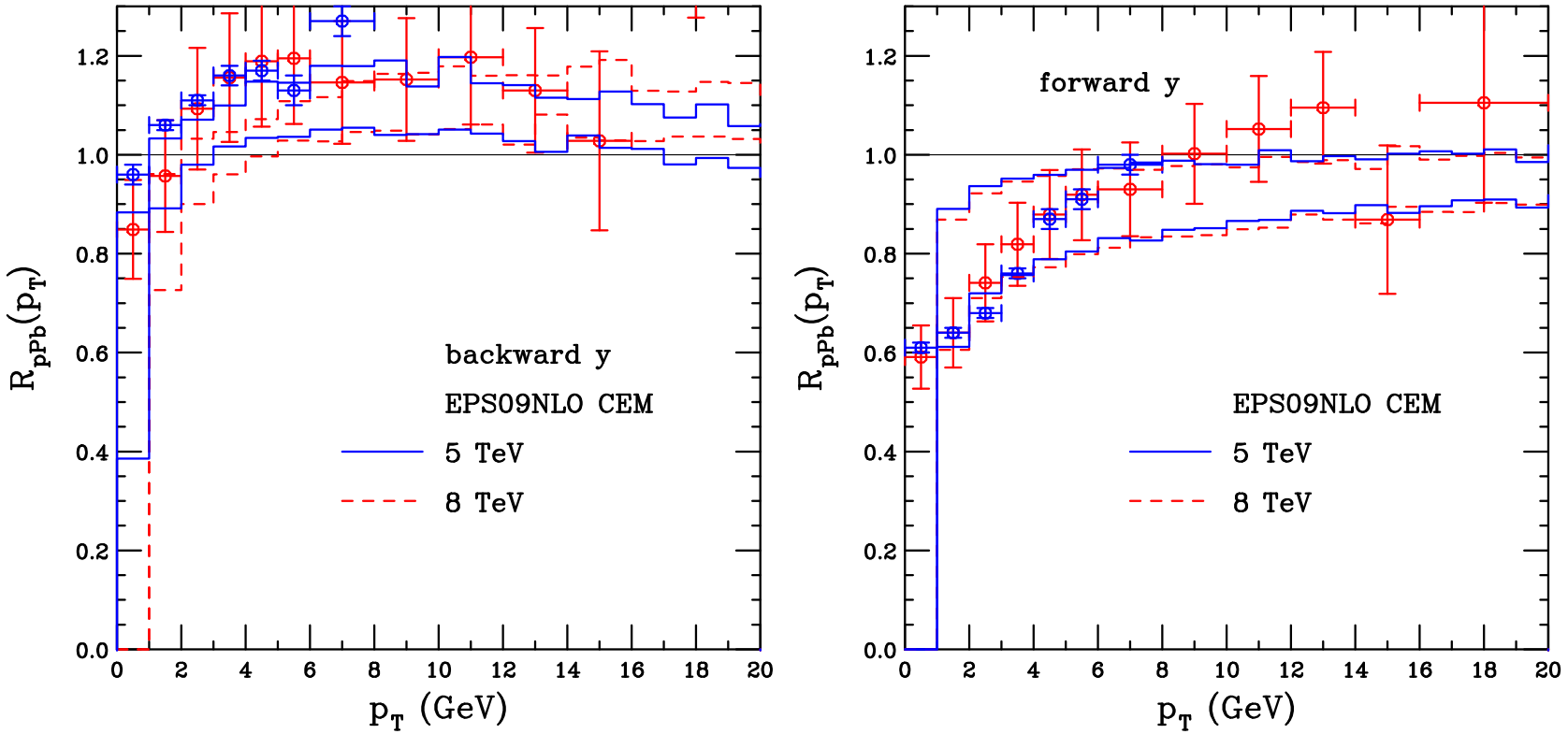

Figure 4: **The ratio $R_{p\mathrm{Pb}}$ for J/ψ as a function of p_T at 5 TeV (blue points and solid blue curves) and 8 TeV (red points and dashes red curves) calculated with EPS09 NLO are compared. The data from ALICE at 5 TeV (JHEP 1402 073) and 8 TeV (JHEP 1807 160) are also shown at backward rapidity (left) and forward rapidity (right).**

$R_{p\mathrm{Pb}}(y)$ for J/ψ: 8.16 TeV

(Left) CEM and data-driven calculations similar for $y > -1$ but CEM uses larger scale in addition to full NLO diagrams

(Middle) Larger uncertainties of nCTEQ and EPS09 LO can accommodate the data; energy loss has right curvature, new HIJING++ does well at forward rapidity

(Right) CGC does well at forward rapidity, larger uncertainty of CGC+NRQCD due to combining of LDME uncertainties separately

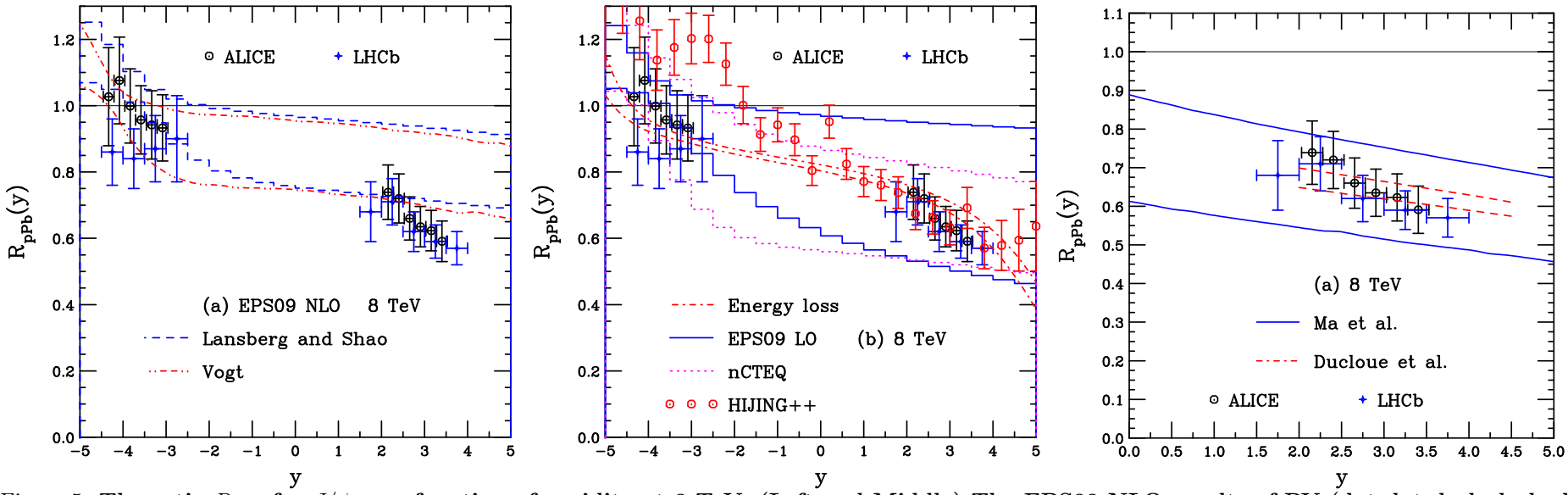

Figure 5: **The ratio $R_{p\mathrm{Pb}}$ for J/ψ as a function of rapidity at 8 TeV. (Left and Middle) The EPS09 NLO results of RV (dot-dot-dash-dashed red curve) and Lansberg and Shao (solid cyan) are shown with their results for EPS09 LO (solid blue histogram) and nCTEQ (dotted magenta histogram) at backward (left) and forward (middle) rapidity. (Right) Results at forward rapidity by Doucloué *et al.* (red dashed curves) and Ma *et al.* in the CGC approach are shown. The ALICE data (JHEP 1807 160) at backward and forward rapidity are shown in black while the LHCb data (PLB 774 (2017) 159) are in blue.**

$R_{p\mathrm{Pb}}(y)$ for J/ψ: 5 vs. 8 TeV

(Left) CEM calculations show a backward shift (entering antishadowing region later) at 8 TeV relative to 5 TeV, unchanged at forward rapidity

(Right) At 8 TeV the energy loss calculation also shows a shift, lower at backward rapidity and higher at forward rapidity, at 8 TeV relative to 5 TeV

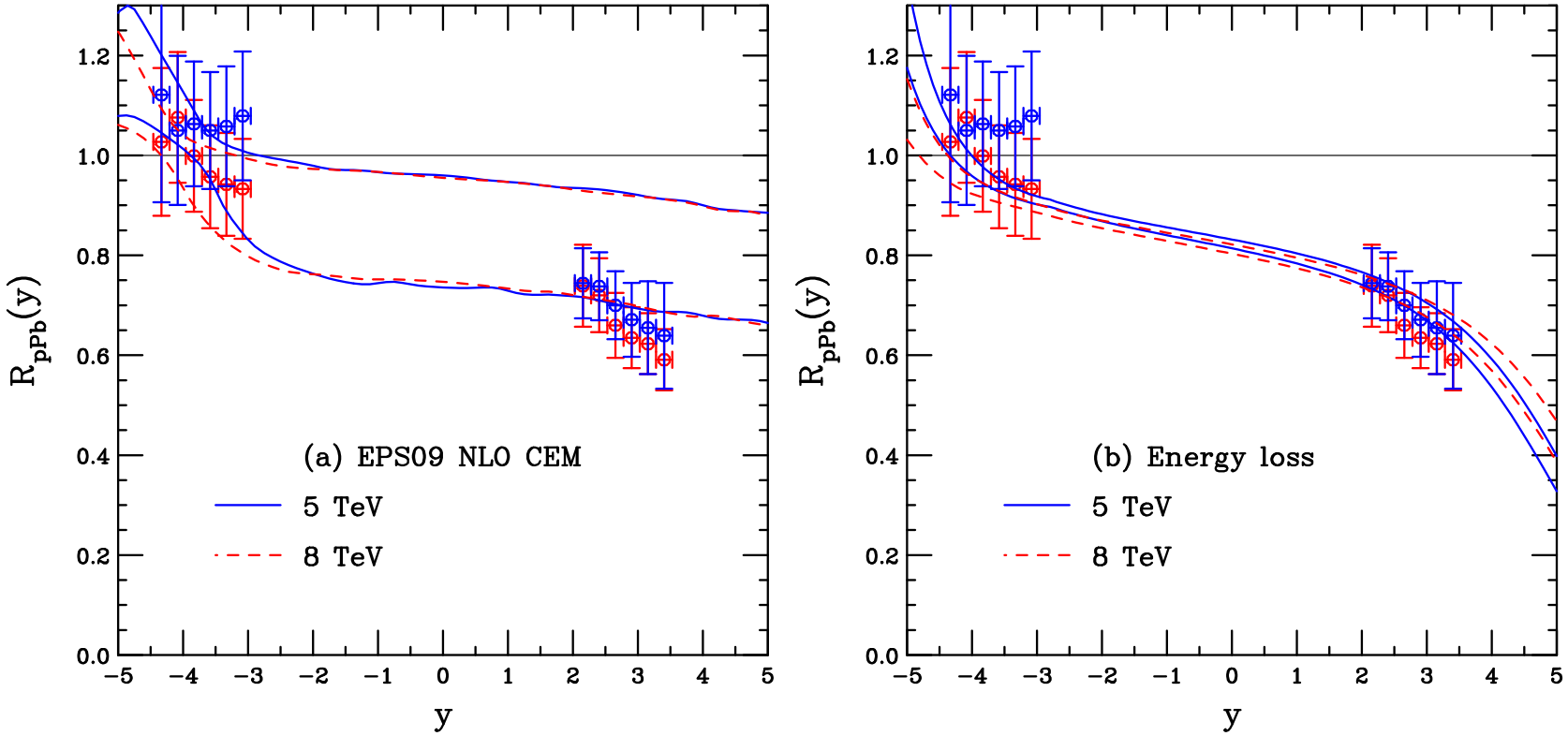

Figure 6: **The ratio $R_{p\mathrm{Pb}}$ for J/ψ as a function of rapidity at 5 TeV (blue points and solid blue curves) and 8 TeV (red points and dashed red curves) are compared. The data from ALICE at 5 TeV (JHEP 1402 073) and 8 TeV (JHEP 1807 160) are also shown. (a) The EPS09 NLO CEM result. (b) The energy loss calculation by Arleo.**

$R_{p\mathrm{Pb}}(y)$ Comover Approach (Ferreiro): 5 TeV

Difference J/ψ and ψ' suppression due to larger ψ' cross section with hadrons, no nucleon absorption, includes EPS09 LO shadowing

$$R^{\psi}_{pA}(b) = \frac{\int \mathbf{d}^2 s\, \sigma_{pA}(b)\, n(b,s)\, S^{sh}_{\psi}(b,s)\, S^{\mathrm{co}}_{\psi}(b,s)}{\int \mathbf{d}^2 s\, \sigma_{pA}(b)\, n(b,s)}$$

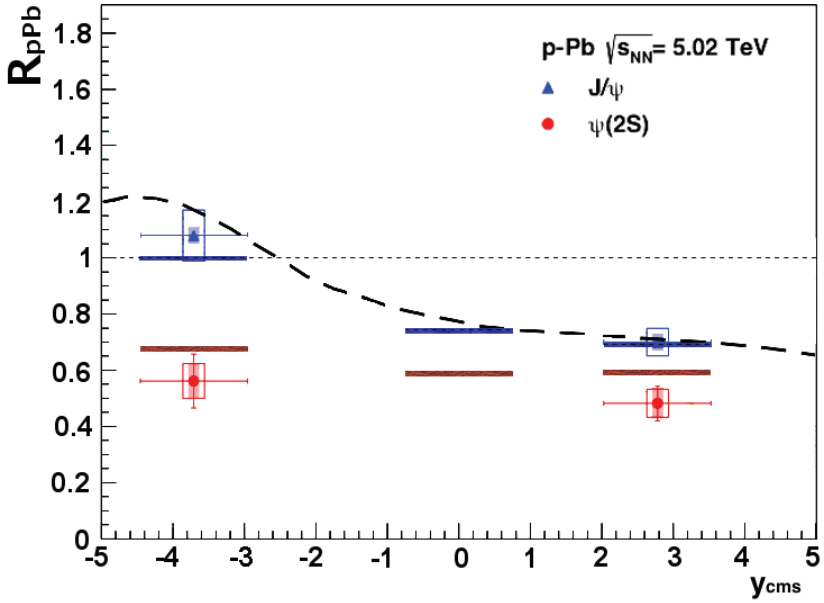

Figure 7: **The J/ψ (blue lines) and $\psi(2S)$ (red lines) nuclear modification factor R_{pPb} as a function of rapidity compared to the ALICE data (JHEP 1412 (2014) 073). The suppression due to shadowing alone (dashed line) is also shown. The ALICE results are given by the points.**

$R_{p\mathrm{Pb}}(y)$ Comover Approach (Ferreiro): 5 TeV vs. 8 TeV

(Left) Further stronger suppression of both J/ψ and ψ(2S) at backward rapidity with higher energy – this difference is almost eliminated at forward rapidity
(Right) Double ratio effect is similar

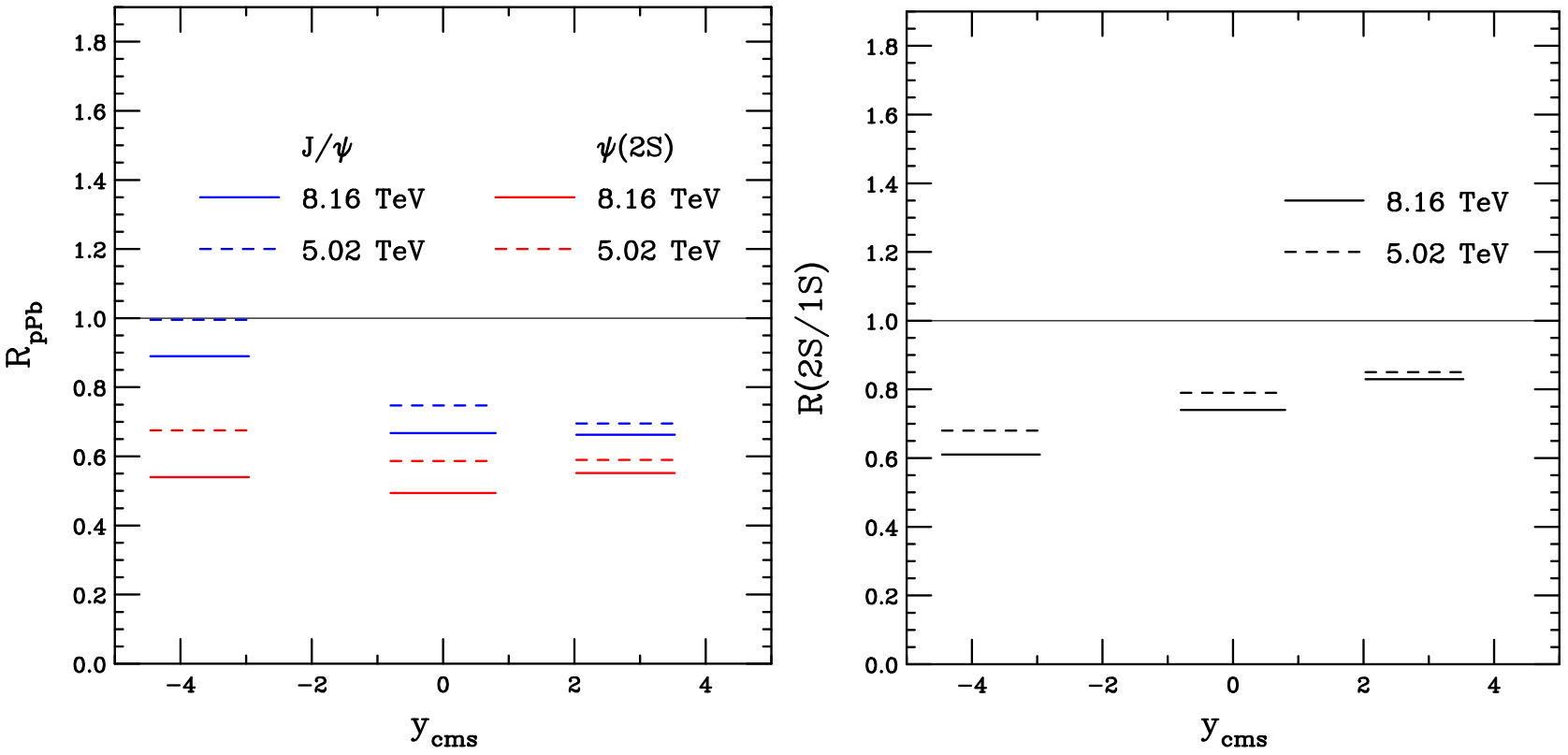

Figure 8: **(Left) The J/ψ (blue lines) and ψ(2S) (red lines) nuclear modification factor $R_{p\mathrm{Pb}}$ as a function of rapidity at 5.02 TeV (dashed lines) and 8.16 TeV (solid lines). (Right) The ratio of nuclear modification factors $R_{p\mathrm{Pb}}(y)$ for ψ(2S) relative to ψ(1S) are compared at 8.16 TeV (solid) and 5.02 TeV (dashed).**

$R_{p\mathrm{Pb}}$ for Υ: 8.16 TeV

No CGC calculations for Υ because scale is higher than Q_{sat} generally

More reduction in $R_{p\mathrm{Pb}}(y)$ at backward rapidity than in the calculations, also at forward rapidity

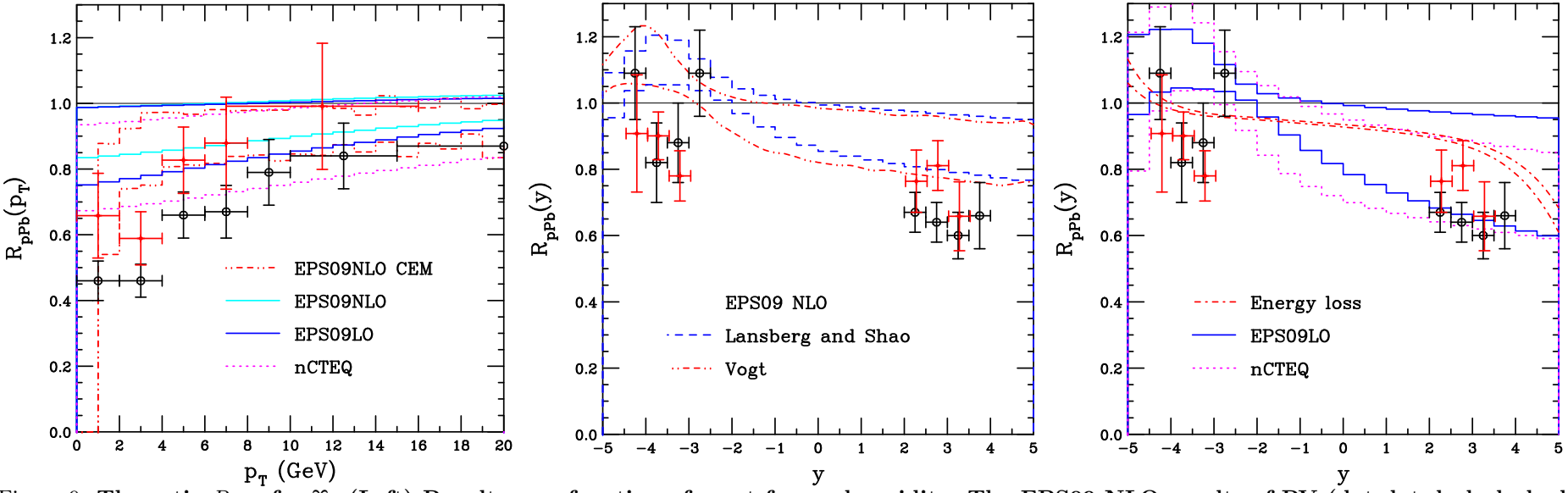

Figure 9: **The ratio R_{pPb} for Υ. (Left) Results as a function of p_T at forward rapidity. The EPS09 NLO results of RV (dot-dot-dash-dashed red curve) and Lansberg and Shao (solid cyan) are shown with their results for EPS09 LO (solid blue histogram) and nCTEQ (dotted magenta histogram). (Middle and Right) Results as a function of rapidity. (Middle) The EPS09 NLO result is compared between the NLO CEM calculation of RV (dot-dot-dash-dashed red curve) and the data-driven result of Lansberg and Shao (solid cyan). (Right) The data-driven calculation of Lansberg and Shao for EPS09 LO (solid blue histogram) and nCTEQ (dotted magenta histogram) is compared to the energy loss only calculation of Arleo (dot-dashed red curve). The LHCb data (JHEP 1811 194) are in black and the preliminary ALICE data are shown in red.**

Predictions for B mesons at 8 TeV

EPS09LO, EPS09NLO and nCTEQ calculations in data-driven approach vs. p_T **and** y

Shadowing, Cronin effect (broadening) and energy loss by Vitev *et al.*

HIJING++ predictions by Barnafoldi *et al.*

Data are LHCb non-prompt J/ψ **and** B^+ **direct**

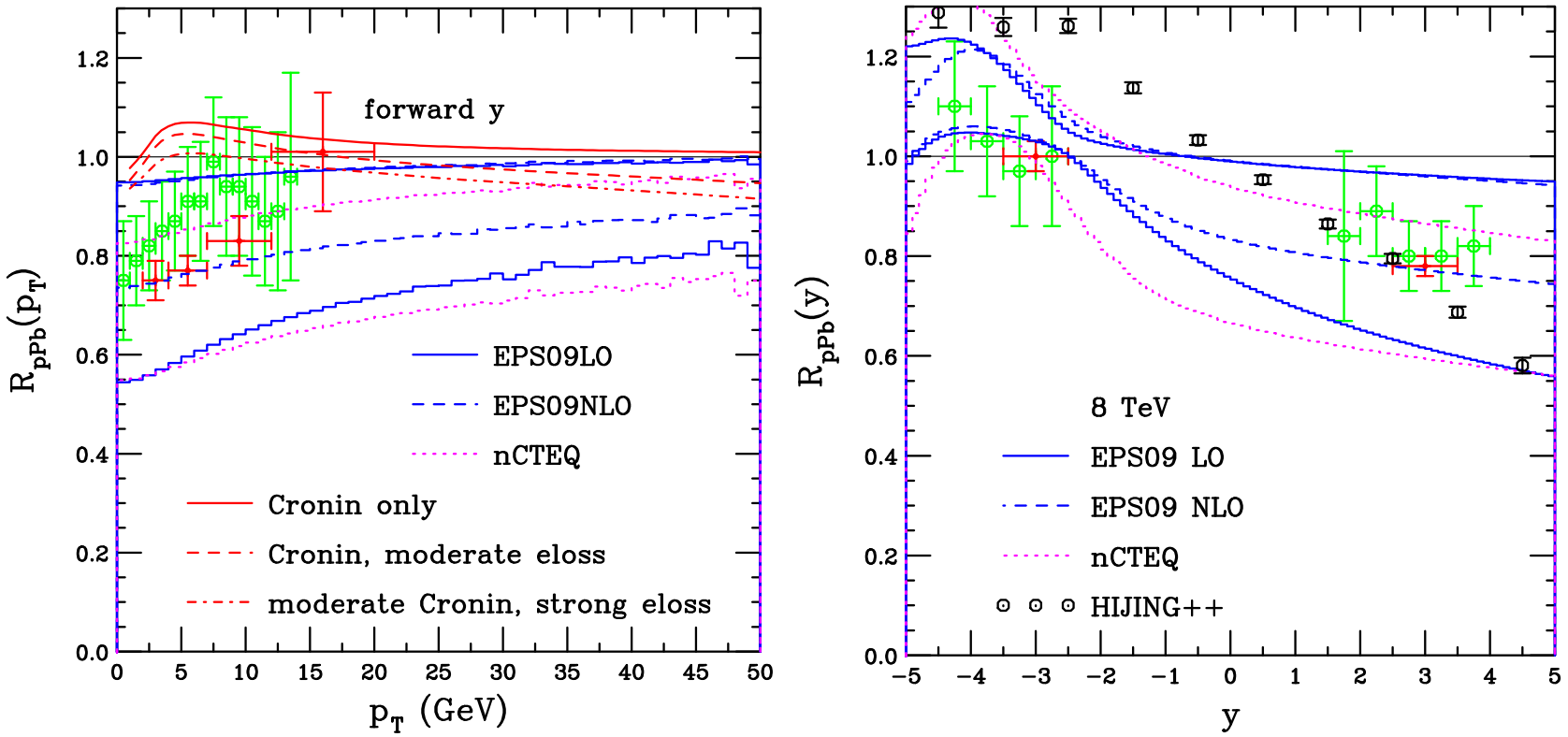

Figure 10: **The calculated** $R_{p\mathrm{Pb}}(y)$ **for the LHC non-promt** J/ψ **(PLB 774 (2017) 159) and** B^+ **(PRD 99 (2019) 052011) data are compared with with EPS09 LO (blue), EPS09 NLO (cyan) and nCTEQ (red) as a function of** p_T **at forward rapidity (left) and as a function of rapidity (right).**

Drell-Yan Production at 8 TeV (Arleo)

Nuclear effects on Drell-Yan production at 8 TeV, shows nuclear effects on the quark distributions

At backward rapidity, neutron-proton number (isospin) appears dominant

Isospin effect small away from antishadowing region where x is smaller and differences between nPDF effects on quark distributions small

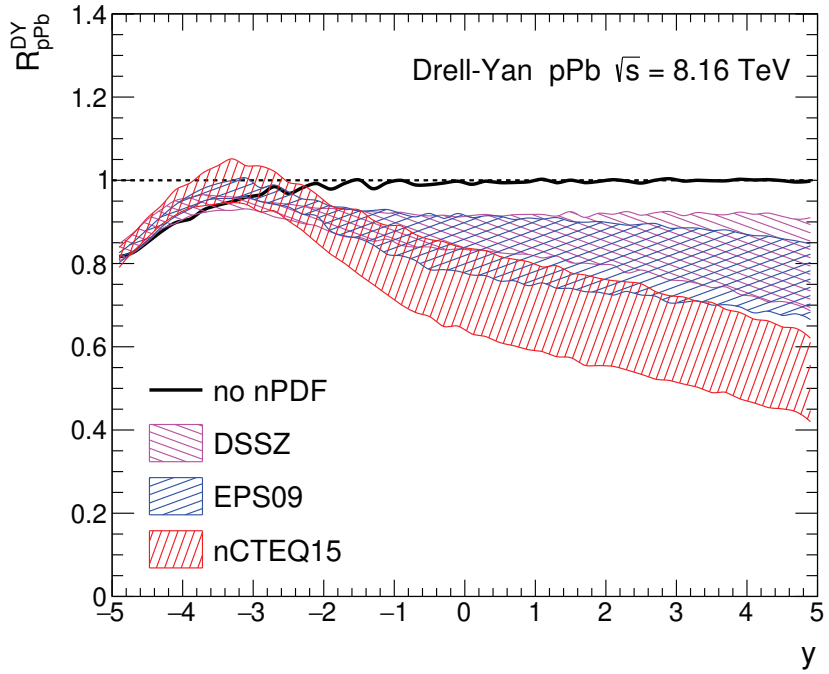

Figure 11: **The calculated $R_{p\mathrm{Pb}}(y)$ for Drell-Yan production with EPS09 NLO (blue), DSSZ (magenta), and nCTEQ15 (red). Albacete *et al.*, in preparation.**

Nuclear Parton Densities

- **All nPDFs are based on collinear factorization**
- **Before LHC turn on, no information about low x and high Q^2 (above 100 GeV^2)**
- **2016 p+Pb run prompted new evaluations of nPDFs, particularly based dijets and gauge bosons**
- **Still no strong constraint on gluon distribution and only lead is probed in this region**
- **Results before and after LHC data are now discussed**

Global Analyses of Nuclear Parton Densities (nPDFs)

Global analyses of nuclear parton densities similar to those of the proton, use same types of data except now the target is a nucleus instead of a proton

Deep inelastic scattering with nuclei showed modifications that depend on momentum fraction, momentum transfer, and nuclear mass, revealing that nucleons in the nucleus are not independent

Global analyses, different than saturation picture, assumes DGLAP evolution and addresses the entire x-range

Types of data employed in global analyses:

- **nuclear deep-inelastic scattering with electrons, muons and neutrinos (not all sets have used neutrino DIS) relative to deuteron or other light target**
- **Drell-Yan data with initial protons (and pions in some cases)**
- **high p_T π^0 production from PHENIX experiment at RHIC**
- **latest sets from Eskola and collaborators also now employs CMS and ATLAS measurements of dijets, Z and $W^{\pm}$ from 5.02 TeV p+Pb run – new regime of high Q^2 and moderate x heretofore unavailable for nPDFs**

Gluon nPDFs directly probed only by dijets and NLO contribution to gauge boson production

Some sets are available for a limited number of interesting targets but some groups have sought to make the sets available for arbitrary A

Previous Parameterizations of Nuclear Parton Densities

EKS98: K. J. Eskola, V. J. Kolhinen and P. V. Ruuskanen, Nucl. Phys. B 535 (1998) 351 [arXiv:hep-ph/9802350]; K. J. Eskola, V. J. Kolhinen and C. A. Salgado, Eur. Phys. J. C 9 (1999) 61 [arXiv:hep-ph/9807297].

EPS09: K. J. Eskola, H. Paukkunen and C. A. Salgado, JHEP 0904 (2009) 065 [arXiv:0902.4154 [hep-ph]].

nDS: D. de Florian and R. Sassot, Phys. Rev. D 69, 074028 (2004) [arXiv:hep-ph/0311227].

DSSZ: D. de Florian, R. Sassot, M. Stratmann and P. Zurita, Phys. Rev. D 85, 074028 (2012) [arXiv:1112.6324 [hep-ph]].

HKN: M. Hirai, S. Kumano and T. H. Nagai, Phys. Rev. C 70, 044905 (2004) [arXiv:hep-ph/0404093].

FGS10: L. Frankfurt, V. Guzey and M. Strikman, Phys. Rept. 512, 255 (2012) [arXiv:1106.2091 [hep-ph]].

EPS09s: I. Helenius, K. J. Eskola, H. Honkanen and C. A. Salgado, JHEP 1207, 073 (2012) [arXiv:1205.5359 [hep-ph]].

nCTEQ15: K. Kovarik *et al.*, Phys.Rev. D 93, 085037 (2016) [arXiv:1509.00792 [hep-ph]].

EPPS16: K. J. Eskola, P. Piakkinen, H. Paukkunen and C. A. Salgado, EPJ C 77 (2017) 163.

Eskola *et al*: EPS09 vs EPPS16

EPPS16

Similar division of nuclear effects on PDFs into x regions

- **shadowing; a depletion at $x \lesssim 0.1$,**
- **anti-shadowing; an excess at $0.1 \lesssim x \lesssim 0.3$,**
- **EMC effect; a depletion at $0.3 \lesssim x \lesssim 0.7$**
- **Fermi motion; an excess towards $x \to 1$ and beyond.**

Define ratios of the individual valence and sea quark distributions and the gluon ratio in nuclei relative to protons

The neutrino DIS, together with $W^{\pm}$ and Z^0 production at the LHC allows separation of the u_V and d_V as well as the $\overline{u}$ and $\overline{d}$ ratios, not possible with only the prior use of Drell-Yan data

This does, however, lead to more parameters overall, 20 instead of 15

$$
\begin{aligned}
R^A_{\bar{q}}(x,Q^2) &\equiv \frac{\bar{q}_A(x,Q^2)}{\bar{q}(x,Q^2)} \quad \bar{q} = \bar{u}, \quad \bar{d}, \quad \bar{s} \\
R^A_{q_V}(x,Q^2) &\equiv \frac{q^A_V(x,Q^2)}{q_V(x,Q^2)} \quad q_V = u_V, \quad d_v \\
R^A_G(x,Q^2) &\equiv \frac{g^A(x,Q^2)}{g(x,Q^2)}
\end{aligned}
$$

Differences Between Eskola *et al* Sets

EKS98: Simple parameterization for all A; leading order analysis only; GRV LO set used for proton PDFs; single set; no χ^2 analysis performed; $2.25 \leq Q^2 \leq 10^4$ GeV^2; $10^{-6} < x < 1$

EPS08: Simple parameterization for all A; leading order analysis only; CTEQ61L set used for proton PDFs; single set; χ^2 analysis uses forward BRAHMS data from RHIC to maximize gluon shadowing; $1.69 \leq Q^2 \leq 10^6$ GeV^2; $10^{-6} < x < 1$

EPS09: Available for only some specific values of A; LO and NLO sets available based on CTEQ61L and CTEQ6M respectively; χ^2 analysis done at both LO and NLO; calling routine similar to other sets but now there are 31, 15 above and 15 below the central set; no longer use BRAHMS data

EPPS16: For the first time, used neutrino DIS and LHC gauge boson and dijet data; use general mass formalism for generating heavy flavor, SACOT; undo experimental isospin corrections in DIS data to have "isoscalar targets"; NLO set only based on CT14NLO; $Q_0^2 = 1.69$ GeV^2

In all cases, when A, x or Q^2 are outside the range of validity, the last value is returned, *e.g.* if $x < 10^{-6}$ value at $x = 10^{-6}$ is given (I believe this is still true for EPPS16, the sets will not be available until after paper is published)

Data Included in EPPS16 Fits (Inclusive of Prior Fits)

Total number of points included, 1811, total χ^2 is 1789

Data sets sorted by mass of heaviest target

CDHSW and NuTeV data not used because no correlations of systematic uncertainties available, CHORUS Pb target has larger neutron excess than Fe so gives more information on flavor separation

For π beams, used GRV pion PDFs

Experiment	Process	Collisions	# points	χ^2
SLAC E139	DIS	e^-He, e^-D	21	12.2
CERN NMC 95, re.	DIS	μ^-He, μ^-D	16	18.4
CERN NMC 95	DIS	μ^-Li, μ^-D	15	18.4
CERN NMC 95, Q^2 dep.	DIS	μ^-Li, μ^-D	153	161.2
SLAC E139	DIS	e^-Be, e^-D	20	12.9
CERN NMC 96	DIS	μ^-Be, μ^-C	15	4.4
SLAC E139	DIS	e^-C, e^-D	7	6.4
CERN NMC 95	DIS	μ^-C, μ^-D	15	9.0
CERN NMC 95, Q^2 dep.	DIS	μ^-C, μ^-D	165	133.6
CERN NMC 95, re.	DIS	μ^-C, μ^-D	16	16.7
CERN NMC 95, re.	DIS	μ^-C, μ^-Li	20	27.9
FNAL E772	DY	pC, pD	9	11.3
SLAC E139	DIS	e^-Al, e^-D	20	13.7
CERN NMC 96	DIS	μ^-Al, μ^-C	15	5.6
SLAC E139	DIS	e^-Ca, e^-D	7	4.8
FNAL E772	DY	pCa, pD	9	3.33
CERN NMC 95, re.	DIS	μ^-Ca, μ^-D	15	27.6
CERN NMC 95, re.	DIS	μ^-Ca, μ^-Li	20	19.5
CERN NMC 96	DIS	μ^-Ca, μ^-C	15	6.4

Experiment	Process	Collisions	# points	χ^2
SLAC E139	DIS	e^-Fe, e^-D	26	22.6
FNAL E772	DY	pFe, pD	9	3.0
CERN NMC 96	DIS	μ^-Fe, μ^-C	15	10.8
FNAL E866	DY	pFe, pBe	28	20.1
CERN EMC	DIS	μ^-Cu, μ^-D	19	15.4
SLAC E139	DIS	e^-Ag, e^-D	7	8.0
CERN NMC 96	DIS	μ^-Sn, μ^-C	15	12.5
CERN NMC 96, Q^2 dep.	DIS	μ^-Sn, μ^-C	144	87.6
FNAL E772	DY	pW, pD	9	7.2
FNAL E866	DY	pW, pBe	28	26.1
CERN NA10*	DY	π^-W, π^-D	10	11.6
FNAL E615*	DY	π^+W, π^-W	11	10.2
CERN NA3*	DY	π^-Pt, π^-H	7	4.6
SLAC E139	DIS	e^-Au, e^-D	21	8.4
RHIC PHENIX	π^0	dAu, pp	20	6.9
CERN NMC 96	DIS	μ^-Pb, μ^-C	15	4.1
CERN CMS*	$W^\pm$	pPb	10	8.8
CERN CMS*	Z^0	pPb	6	5.8
CERN ATLAS*	Z^0	pPb	7	9.6
CERN CMS*	dijet	pPb	7	5.5
CERN CHORUS*	DIS	νPb, $\overline{\nu}$Pb	824	998.6

Table 1: **The data sets used in the analyses. The reactions are given for each specific case. The number of data points given are only those that satisfy the kinematic cuts, $Q^2, M^2 \geq 1.69\,\mathrm{GeV}^2$ for DIS and DY, and $p_T \geq 2\,\mathrm{GeV}$ for hadron production at RHIC. Only these points contribute to the χ^2 of each set. The data added since the EPS09 analysis are marked with a star. Eskola *et al*, arXiv:1612.05741 [hep-ph].**

Comparison of x, Q^2 Ranges of EPS09NLO and EPPS16

Note the difference in the x and y axes scales – EPPS16 plot does not show data below $Q^2 = 1$ GeV^2

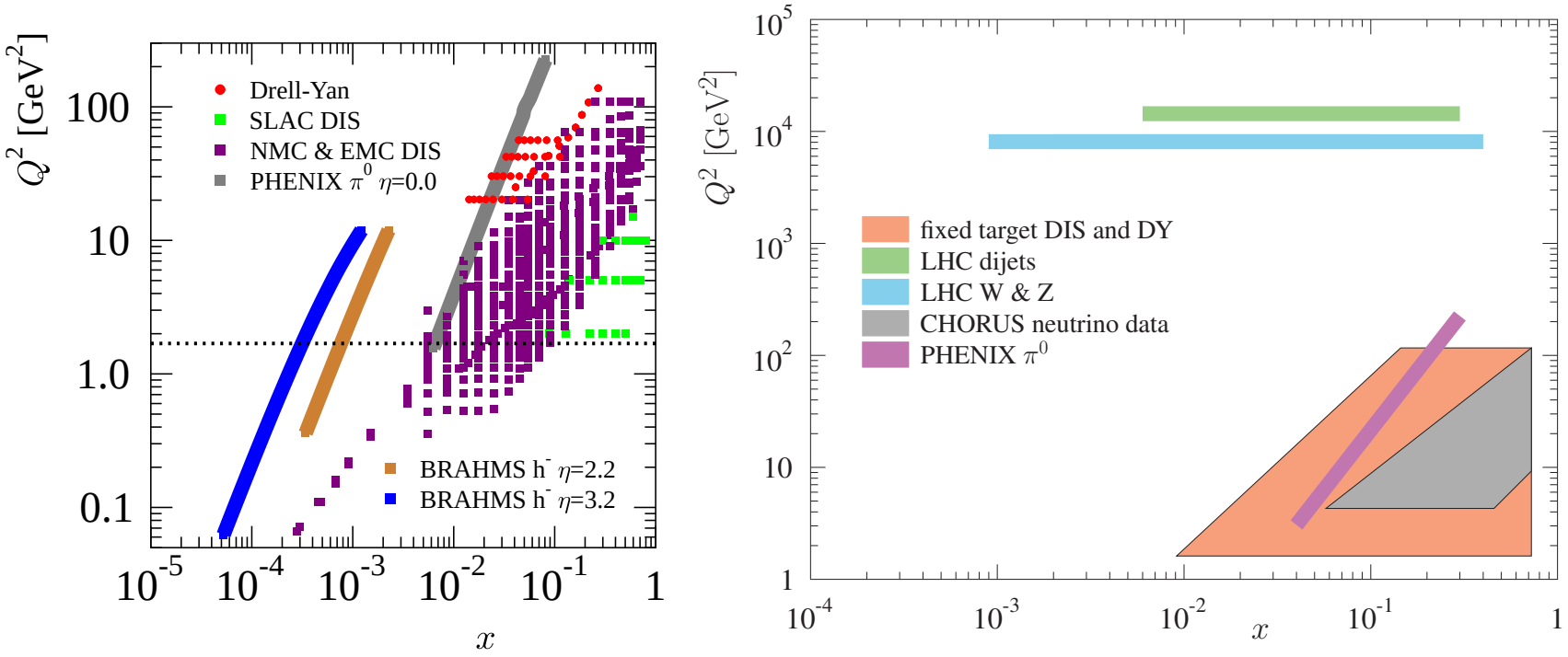

Figure 12: **Left: Data included for EPS09, JHEP 0904 (2009) 065. Right: Data included for EPPS16. Eskola *et al*, EPJ C 77 (2017) 163.**

EPPS16 Parameterization

Similar parameterizations but now for $i = u_V, d_V, \overline{u}, \overline{d}, s$, and g

$$R_i^A(x) = \begin{cases} a_0 + a_1(x - x_a)^2 & x \le x_a \\ b_0 + b_1 x^\alpha + b_2 x^{2\alpha} + b_3 x^{3\alpha} & x_a \le x \le x_e \\ c_0 + (c_1 - c_2 x)(1 - x)^{-\beta} & x_e \le x \le 1, \end{cases}$$

y_0	**Maximum shadowing effect as $x \to 0$**
x_a, y_a	**Position, height of antishadowing maximum, $\alpha = 10x_a$**
x_e, y_e	**Position, height of the EMC minimum**
$\beta = 1.3$	**Slope in the Fermi-motion part**
$y_i(A) = y_i(A_C)\left(\frac{A}{A_C}\right)^{\gamma_i[y_i(A_C)-1]}$	**A dependence of fit parameters relative to $A_C = 12$**

a_i, b_i, c_i fixed from minimia and maxima at $y_0 = R_i^A(x \to 0, Q_0^2)$, $y_a = R_i^A(x_a, Q_0^2)$ and $y_e = R_i^A(x_e, Q_0^2)$, continuity and vanishing first derivatives at matching points x_a, x_e

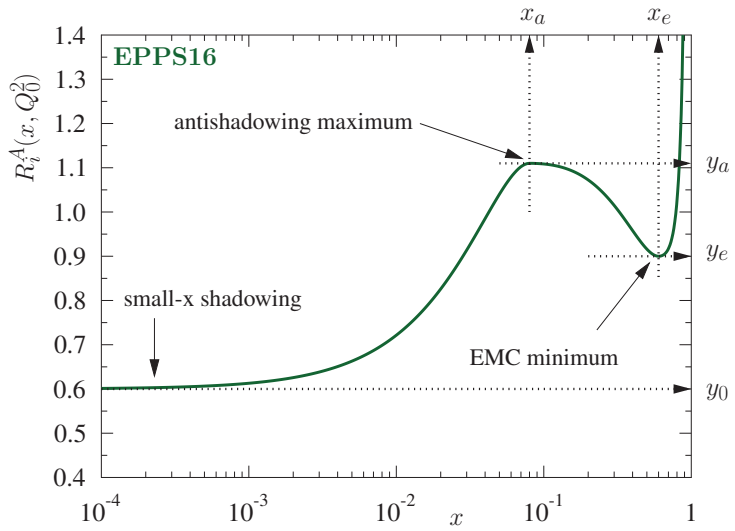

Figure 13: **An illustration of the fit function $R_i^A(x)$ and the role of the parameters x_a, x_e, y_0, y_a, and y_e.**

Fitting Procedure

Define a local χ^2 based on N data sets and a given input parameter set to be varied, $\{a\}$, with χ^2_N for each data set

Set of weight factors w_N used to amplify the importance of χ^2_N to the fit for sets that have large influence but small relative χ^2

$$\begin{aligned}\chi^2(\{a\}) &\equiv \sum_N w_N\,\chi^2_N(\{a\}) \\ \chi^2_N(\{a\}) &\equiv \left(\frac{1-f_N}{\sigma_N^{\rm norm}}\right)^2 + \sum_{i\in N}\left[\frac{f_N D_i - T_i(\{a\})}{\sigma_i}\right]^2,\end{aligned}$$

D_i are data points with a σ_i point-to-point uncertainty (statistical and systematic uncertainties added in quadrature), f_N is normalization factor for sets with relative normalization uncertainty $\sigma_N^{\rm norm}$ fixed each iteration by minimizing χ^2_N for each parameter set $\{a\}$, T_i is calculated value to be compared to $f_N D_i$

Weak constraint on low x gluons so to cure unwanted parameter drift into unphysical region with stronger shadowing at small A, introduce penalty

$$1000\left[\left(y_0^G({\rm He}) - y_0^G({\rm Pb})\right) - \left(y_0^S({\rm He}) - y_0^S({\rm Pb})\right)\right]^2$$

If χ^2-minimized set of parameters, $\{a_0\}$, gives best estimate of nPDFs, work in a basis $\{z\}$ that diagonializes covariance matrix, errors in nPDFs computed within 90% confidence criteria, $\Delta\chi^2 = 50$

Upper and lower uncertainties on observable X computed using prescription

$$\begin{aligned}(\Delta X^+)^2 &\approx \sum_k \left[\max\left\{X(S_k^+) - X(S^0), X(S_k^-) - X(S^0), 0\right\}\right]^2 \\ (\Delta X^-)^2 &\approx \sum_k \left[\max\left\{X(S^0) - X(S_k^+), X(S^0) - X(S_k^-), 0\right\}\right]^2\end{aligned}$$

Q^2 Dependence of EPPS16

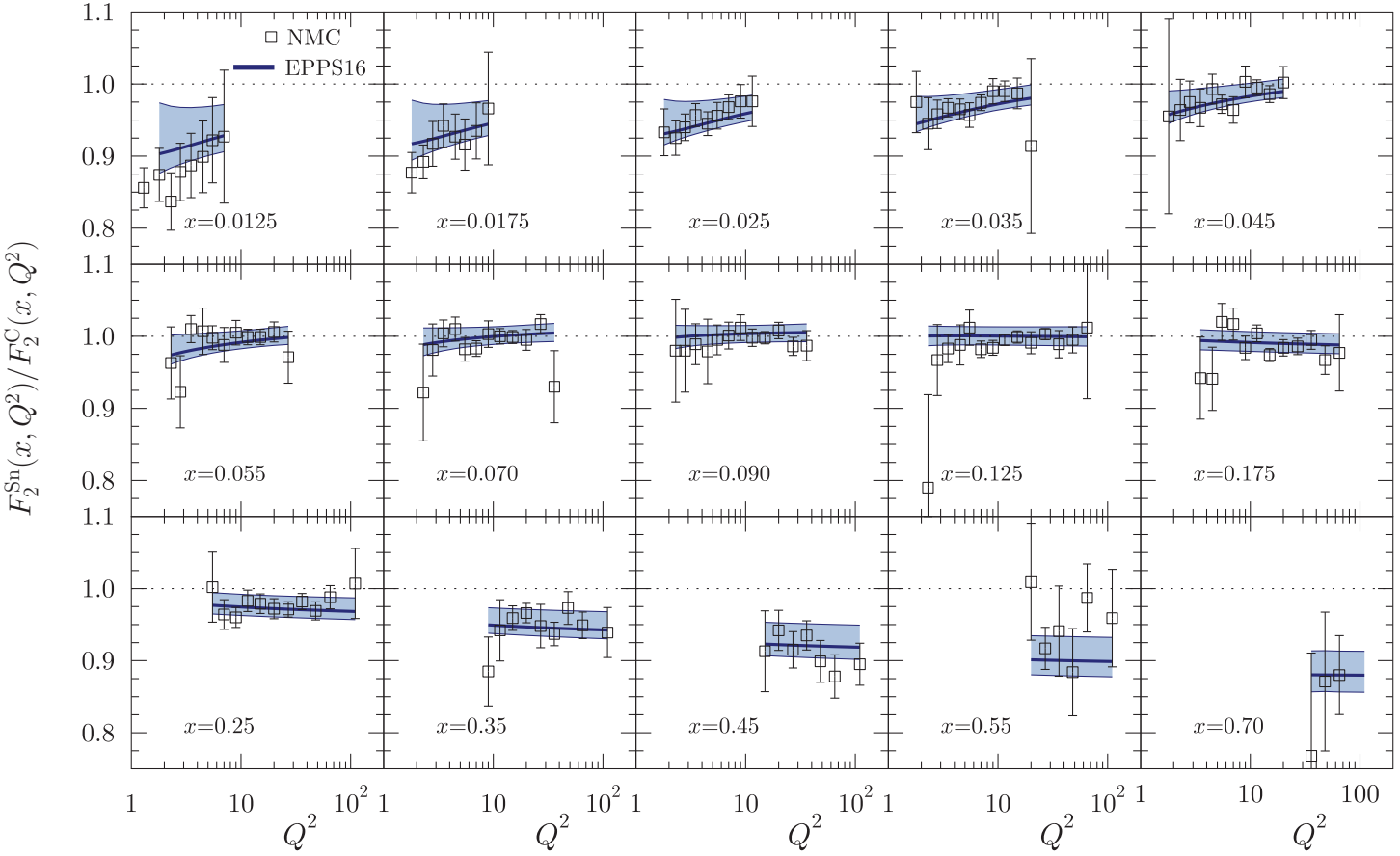

Figure 14: **Evolution of $F_2^{\mathrm{Sn}}/F_2^{\mathrm{C}}$ with Q^2 for different values of x with EPPS16. Eskola *et al*, EPJ C 77 (2017) 163.**

x Dependence of EPPS16

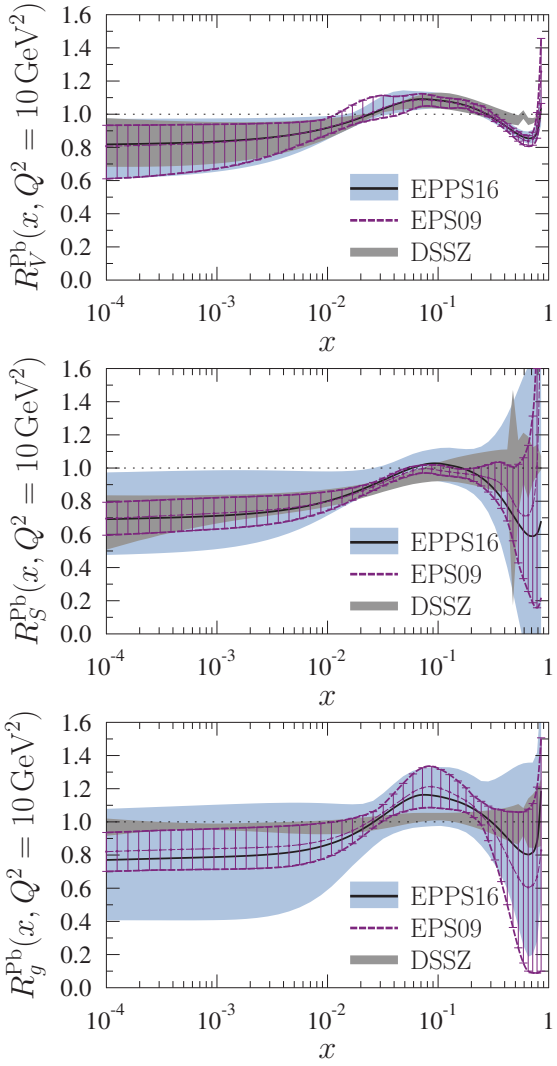

Figure 15: **The x dependence of the average valence (left), sea (center), and gluon (right) distributions for $Q^2 = 10$ GeV^2. EPPS16 (blue-gray band) is compared to EPS09NLO (red band) and DSSZ (dark-gray band). Eskola *et al*, EPJ C 77 (2017) 163.**

Dijets

First truly large x and Q^2 probe of the gluon distribution in the nucleus

Dijets with EPS09 NLO at 5.02 TeV

Rapidity distribution (Eskola *et al*) shows clear shift relative to proton PDFs alone

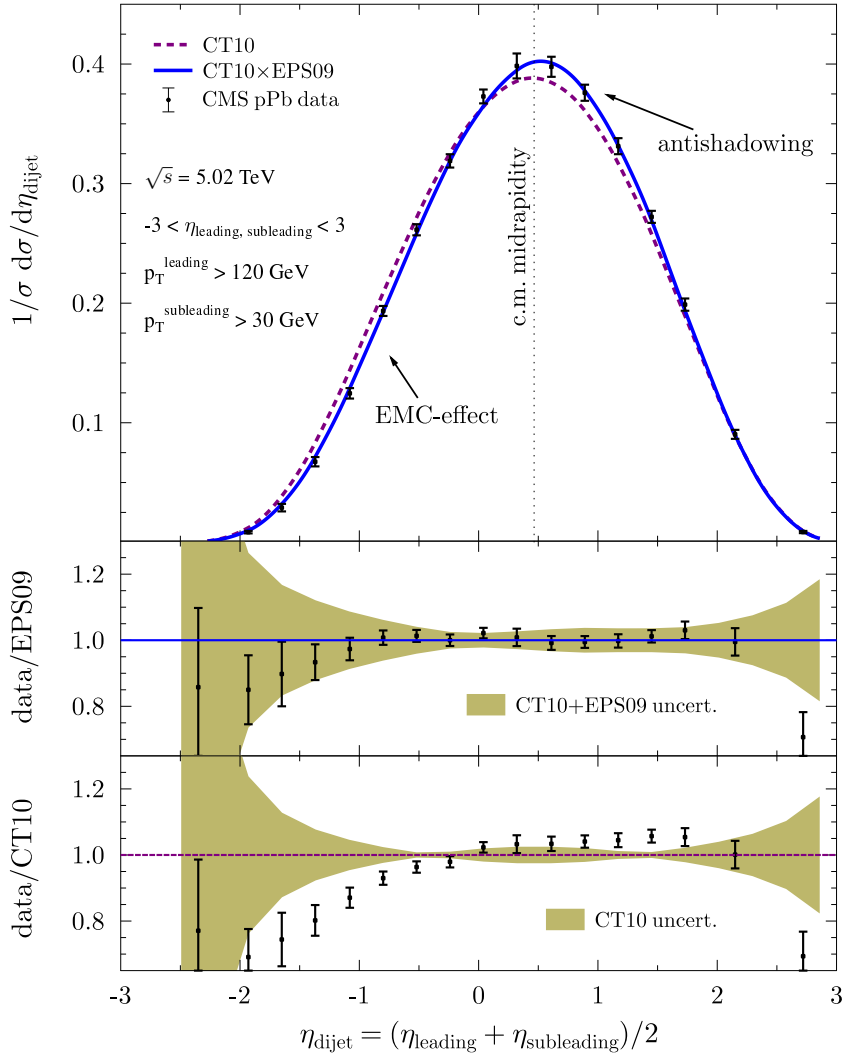

Figure 16: **The CMS dijet measurements (Eur. Phys. J. C 74 (2014) 2951) are compared to EPS09 NLO. The upper panel shows the normalized cross section as a function of η_{dijet}. The lower two panels display the ratio of the data to the CT10+EPS09 and CT10 calculations respectively, including the PDF and nPDF uncertainty bands.**

x Range in different p_T regions

Rapidity distribution (Eskola *et al*) shows clear shift

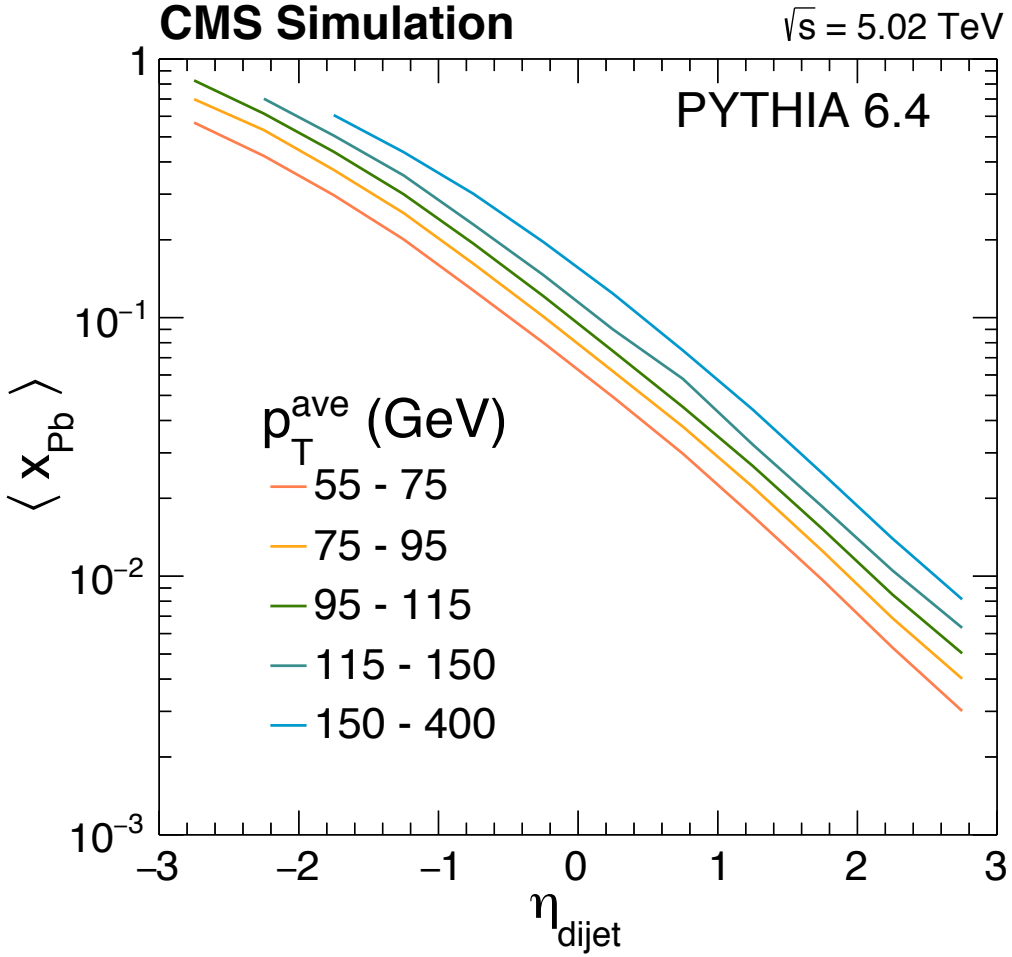

Figure 17: **PYTHIA simulations of the x range probed by dijets in CMS as a function of rapidity andd p_T intervval. (CMS, PRL 121 (2018) 062002)**

Data compared to EPS09 and DSSZ in several p_T ranges

Small gluon shadowing of DSSZ ruled out, too weak
EPS09 agrees best with lowest p_T bin, underestimates forward rapidity

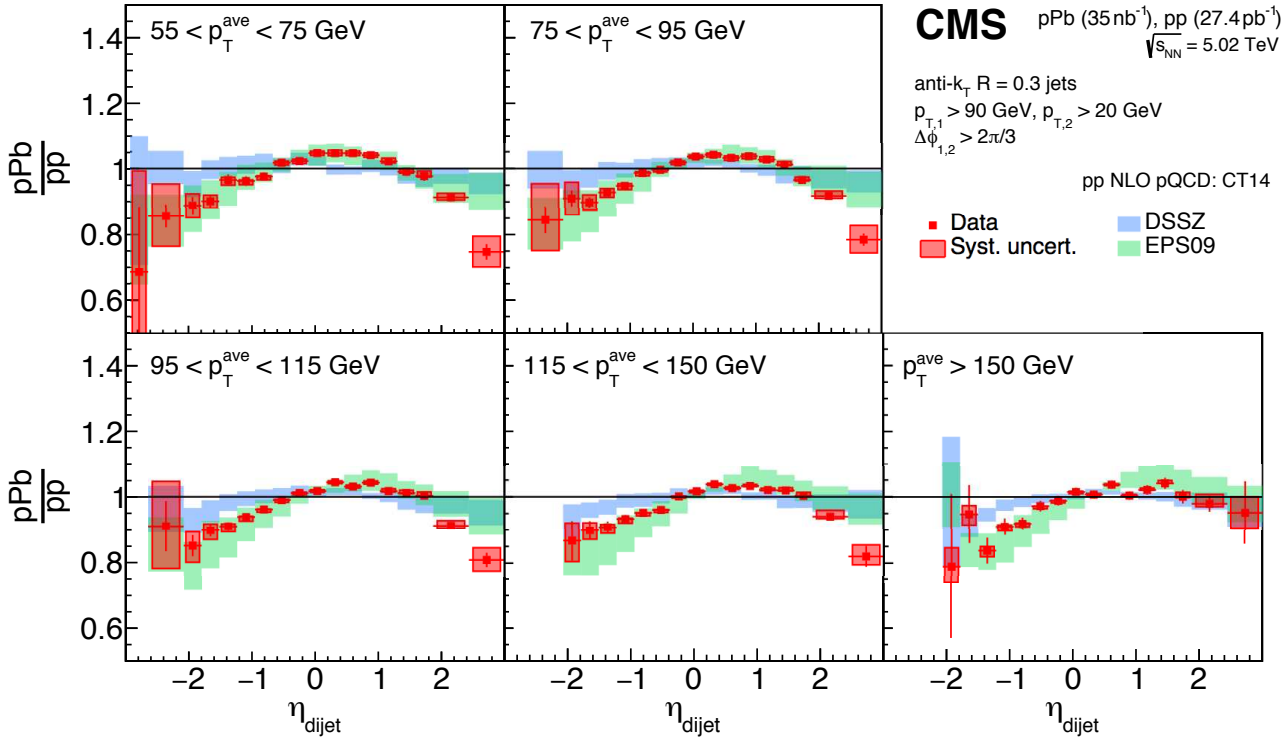

Figure 18: **The CMS dijet measurements are compared to EPS09 (green) and DSSZ (blue) calculations in five different p_T bins. (CMS, PRL 121 (2018) 062002)**

Data over Theory before and after EPPS16

Average p_T range of $115 < p_T^{\mathrm{ave}} < 150$ GeV is shown

nPDFs before LHC measurements all show some discrepancy relative to data at backward rapidity and in most forward rapidity bins
EPPS16, including these data improves the agreement, as it should

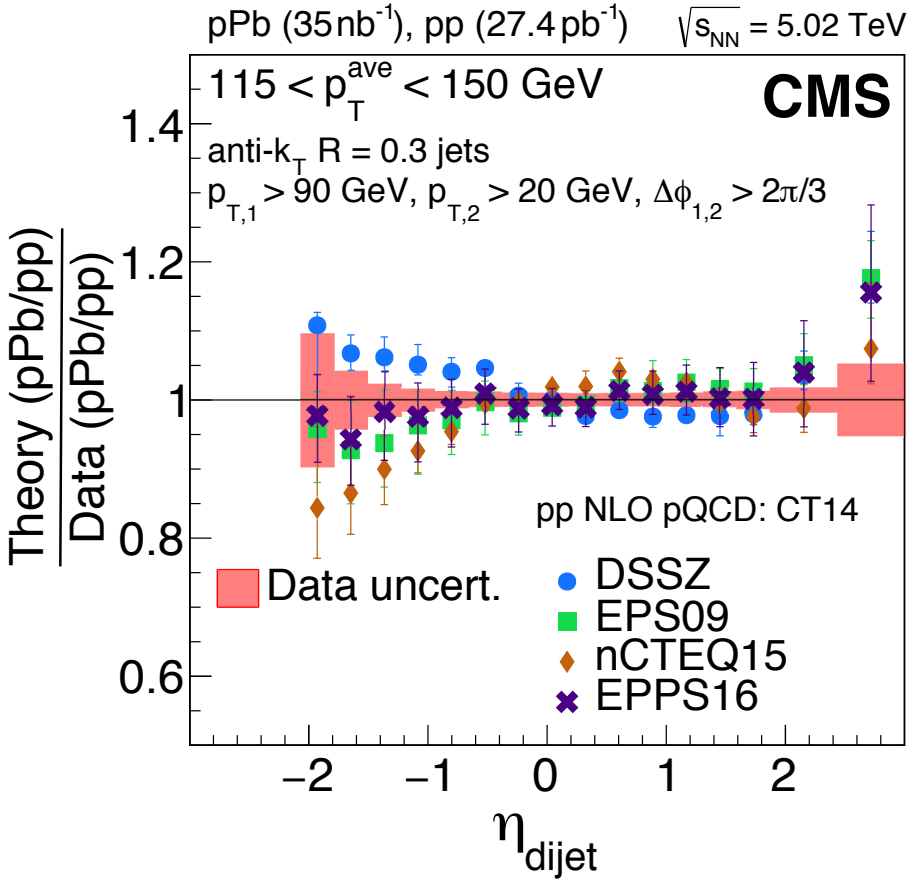

Figure 19: **Double ratio of pPb/pp ratio for theory relative to data for $115 < p_T^{\mathrm{ave}} < 150$ GeV with DSSZ (blue), EPS09 (green), nCTEQ15 (brown) and EPPS16 (black) (CMS, PRL 121 (2018) 062002)**

Dijets in CMS at 5.02 TeV: Forward-Backward Asymmetry

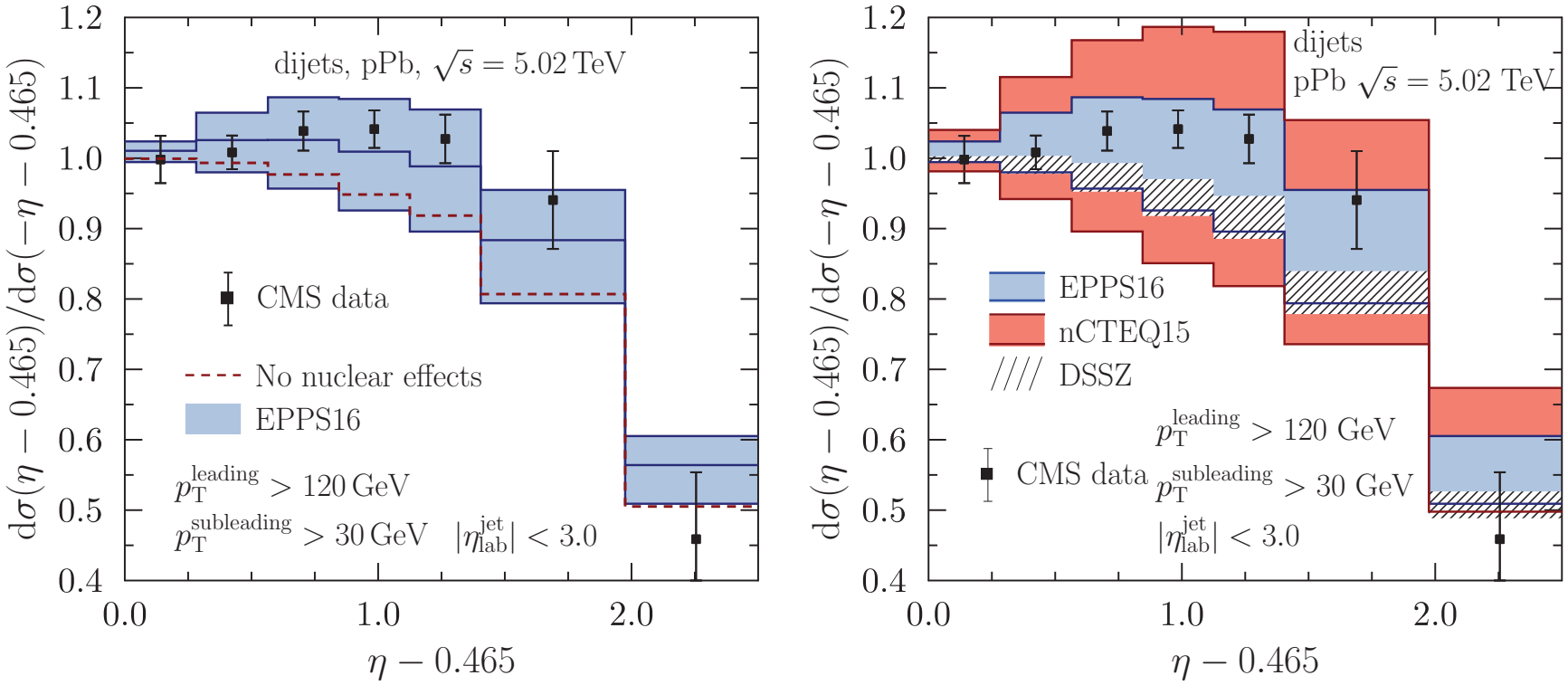

Figure 20: **Left: Dijet production with EPPS16 compared to no nuclear effects, isospin only. Right: EPPS16 results are compared to nCTEQ and DSSZ. Eskola *et al*, EPJ C 77 (2017) 163.**

Gauge Bosons

Excellent probes of quark and antiquark distributions at large Q^2 and moderate x, especially $W^{\pm}$

W^+, W^- and Z^0 rapidity distributions: 5.02 TeV

Calculations by Ru *et al.*, PRD 94, 113013 (2016), also appearing in Albacete *et al.*

Employ EPS09 and Kulagin-Petti nPDFs, also compared to results with no nPDF modification

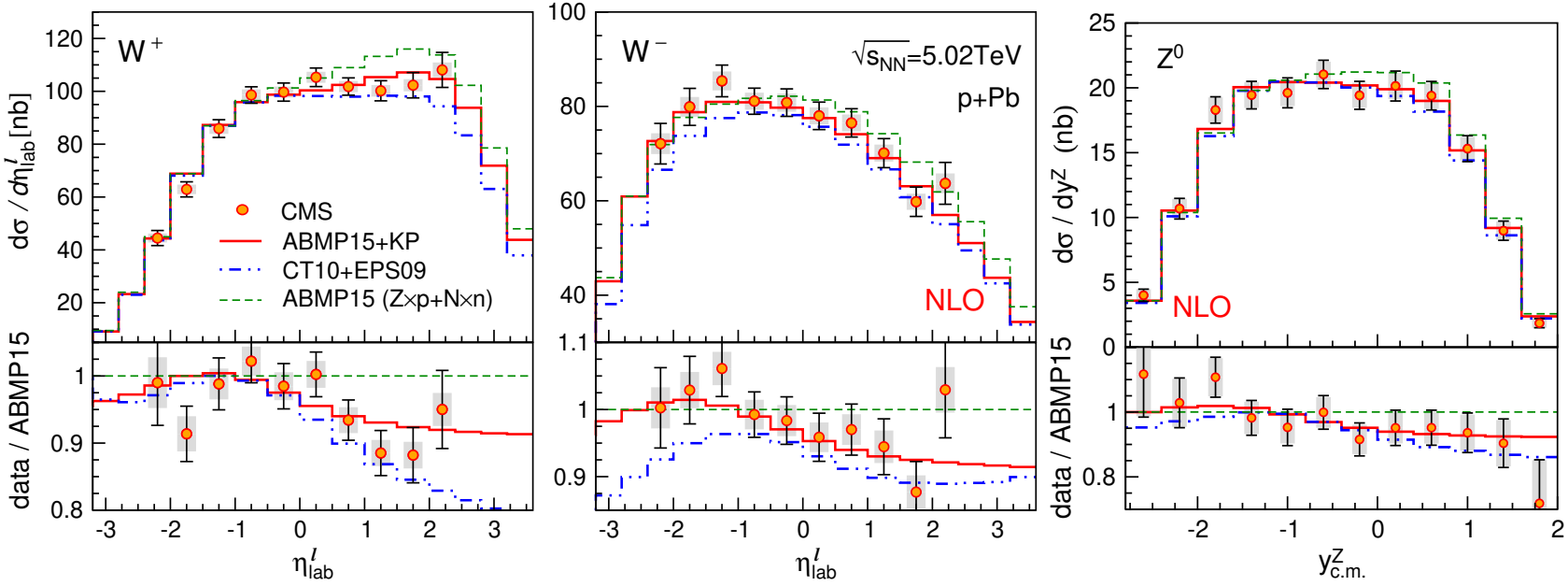

Figure 21: **Calculation of W^+ (left), W^- (middle) and Z^0 (right) rapidity distributions, measured through their lepton decays. Ratios relative to calculations with no nuclear effects are also shown. From Ru *et al.*, and also in Albacete *et al.*, Int. J. Mod. Phys. E 25 (2016) 1630005.**

Forward-backward asymmetries in W^+, W^-, and Z^0 production: 5.02 TeV

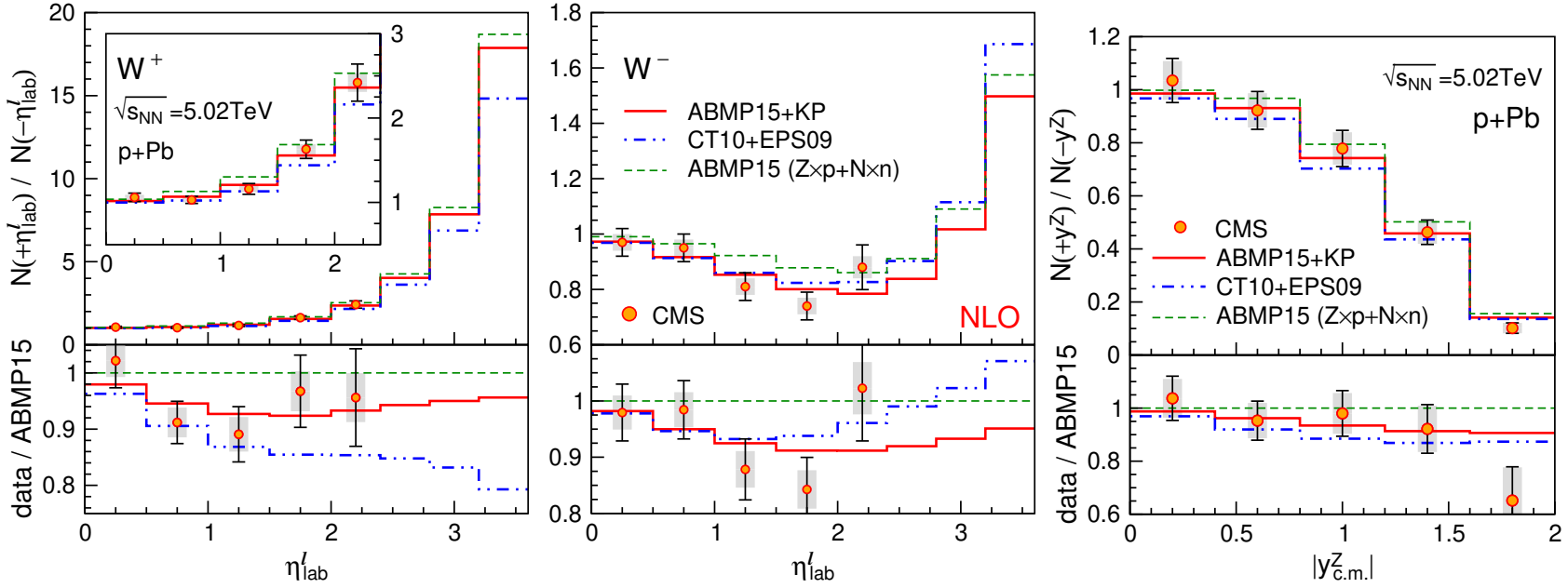

Figure 22: **Calculation of W^+ (left), W^- (middle) and Z^0 (right) forward-backward asymmetries, measured through their lepton decays. Ratios relative to calculations with no nuclear effects are also shown. From Ru *et al.*, and also in Albacete *et al.*, Int. J. Mod. Phys. E 25 (2016) 1630005. The CMS $W^\pm$ data are from PLB 750 (2015) 565 while the Z^0 data are from PLB 759 (2016) 36.**

W^+, W^- Asymmetries: EPPS16

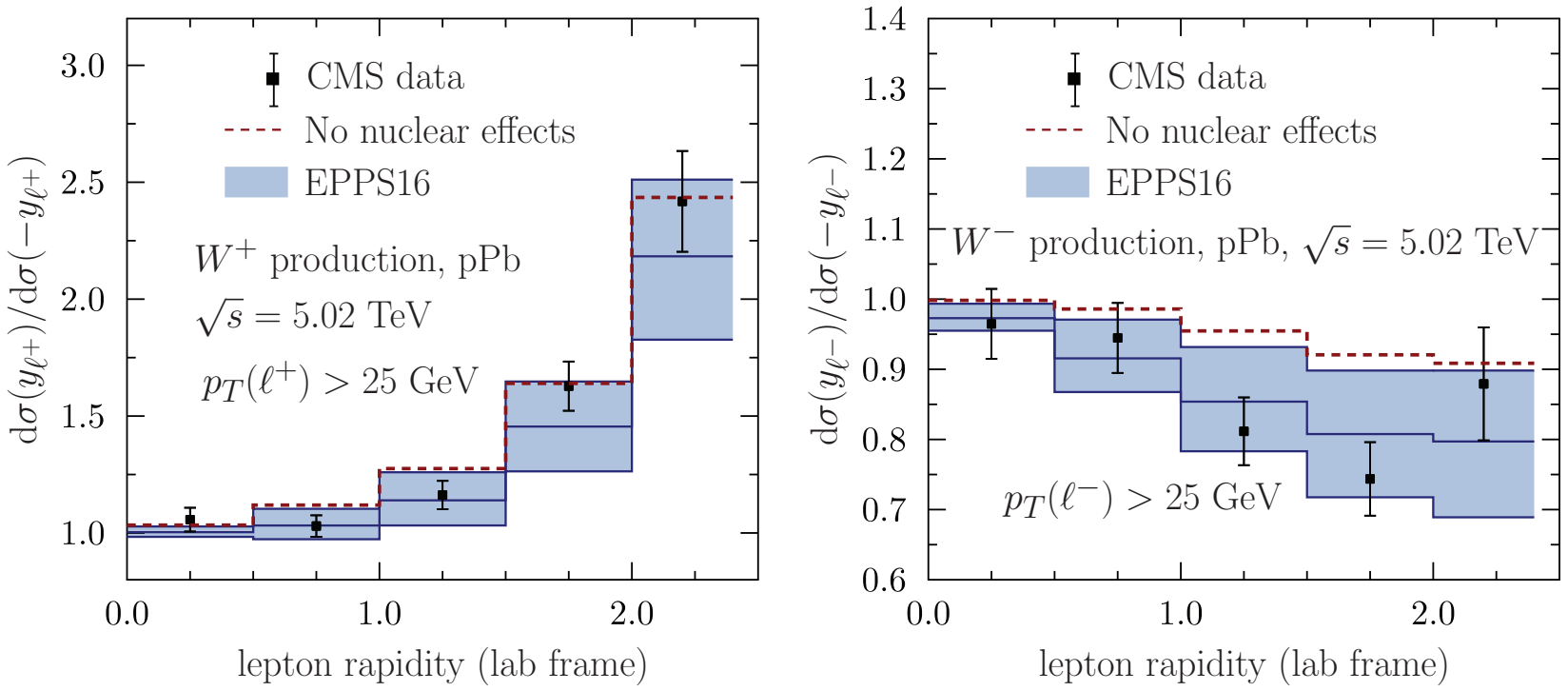

Figure 23: **Lepton forward-backward asymmetry for W^+ (left) and W^- (right) with EPPS16. Eskola *et al*, EPJ C 77 (2017) 163. The CMS data are from PLB 750 (2015) 565.**

W^+, W^- Charge Asymmetry: 5.02 TeV

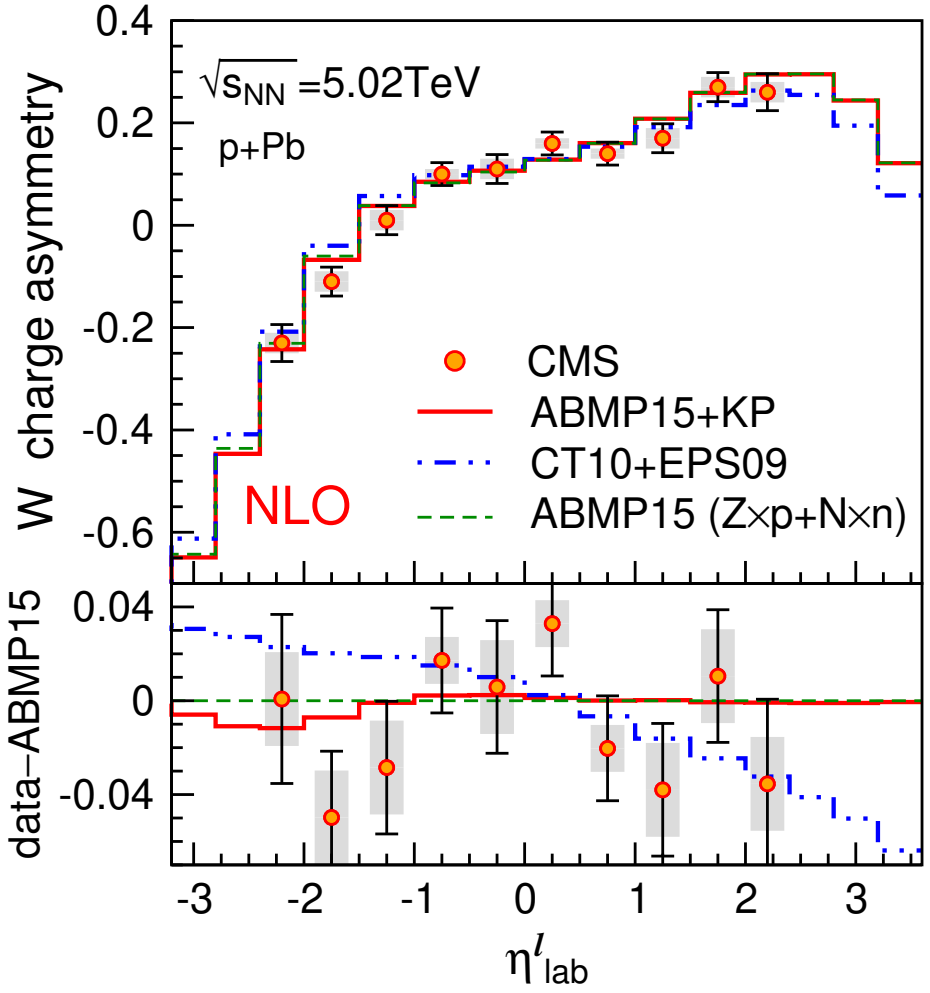

Figure 24: **Calculation of W^+, W^- charge asymmetry as a function of rapidity, measured through their lepton decays. Ratios relative to calculations with no nuclear effects are also shown. From Ru *et al.*, and also in Albacete *et al.*, Int. J. Mod. Phys. E 25 (2016) 1630005. The CMS data are from PLB 750 (2015) 565.**

W^+ and W^- rapidity distributions: 8.16 TeV

New CMS 8 TeV data show clear preference for EPPS16d over no effect or older ses lika nCTEQ15 for both W^+ and W^- production
This preference was already clear from 5 TeV data

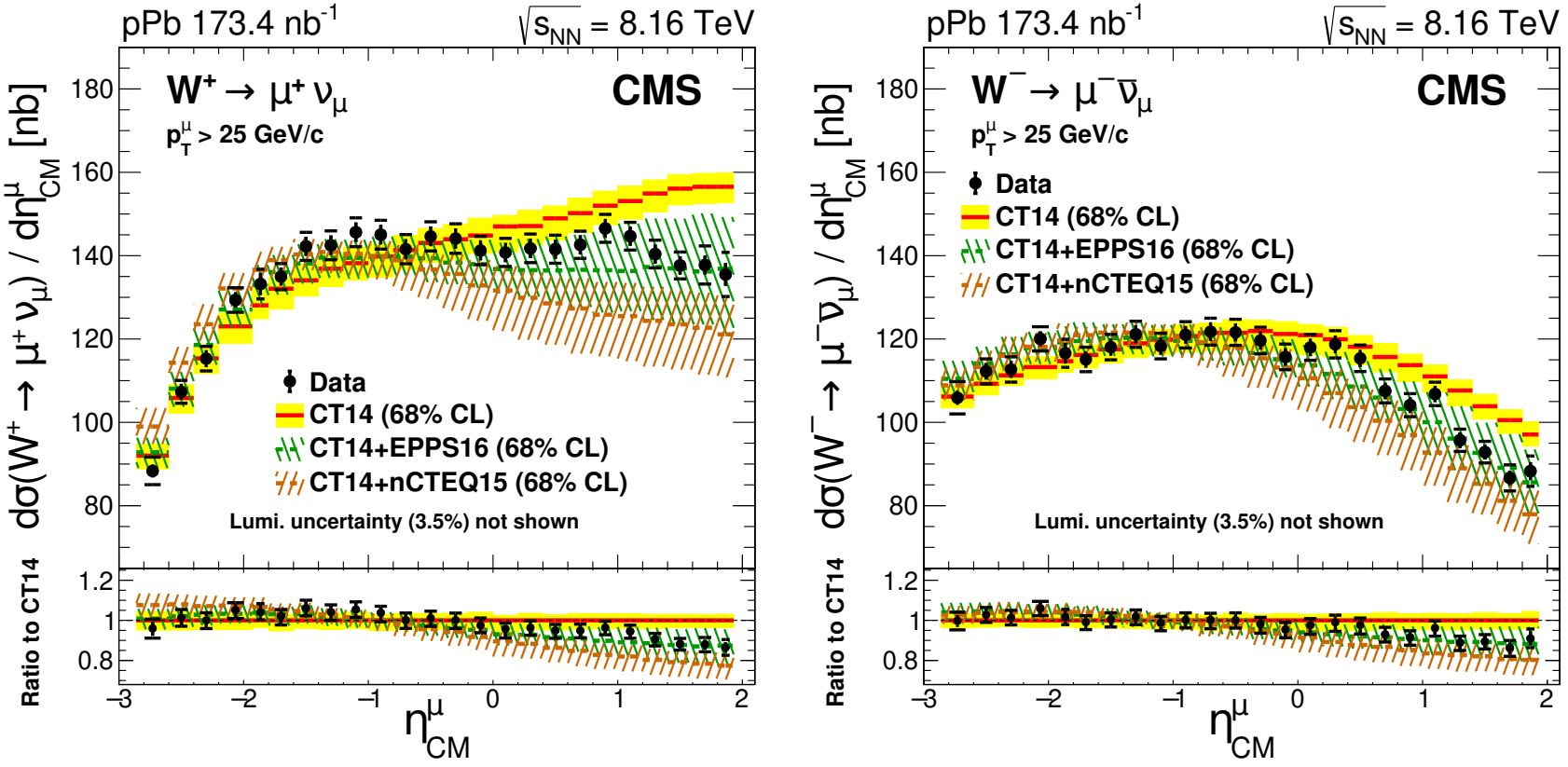

Figure 25: **CMS measurement of W^+ (left) and W^- (right) rapidity distributions through their lepton decays. Ratios relative to calculations with no nuclear effects are also shown. From arXiv:1905.01486 [hep-ex]. See also Albacete *et al.*, NPA for predictions by Ru *et al.*.**

Forward-backward asymmetries in W^+ and W^- production: 8.16 TeV

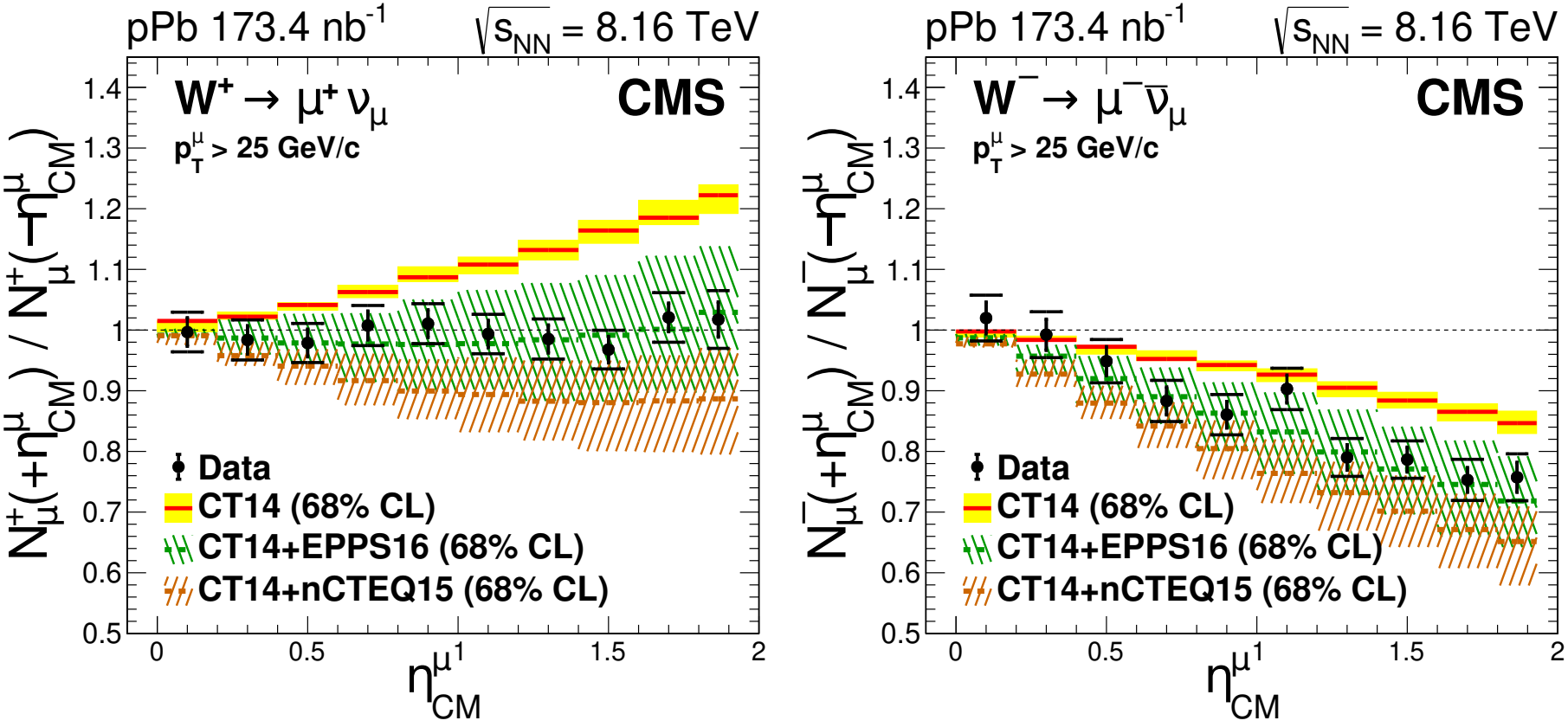

Figure 26: **Calculation of W^+ (left), W^- (middle) and Z^0 (right) forward-backward asymmetries, measured through their lepton decays. Ratios relative to calculations with no nuclear effects are also shown. From arXiv:1905.01486 [hep-ex]. See also Albacete *et al.*, NPA for predictions by Ru *et al.*.**

W^+, W^- Charge Asymmetry: 8.16 TeV vs 5 TeV)

Charge asymmetry is less discriminatory than individual distributions for CNM effects

Little to no significant difference between energies

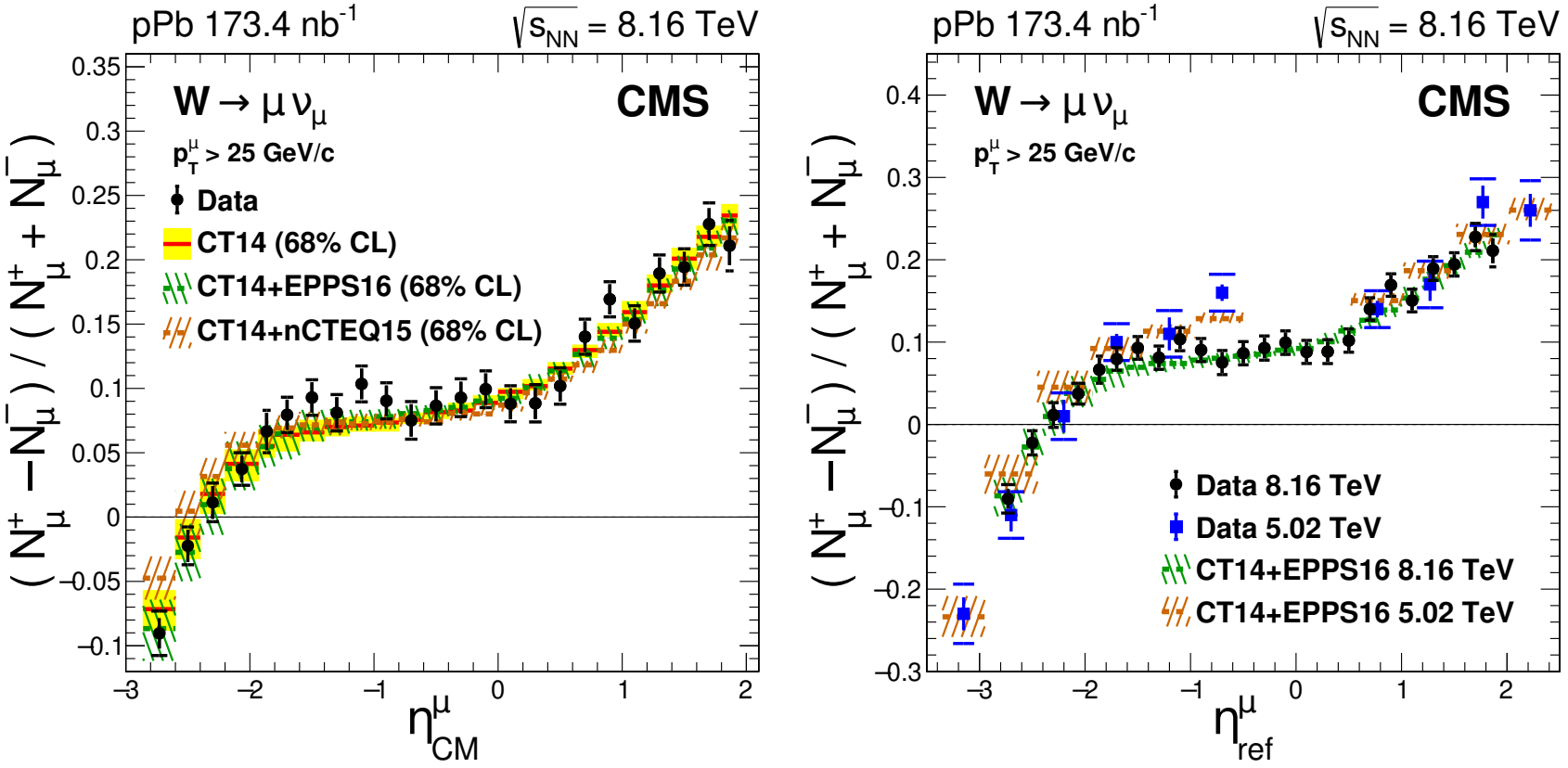

Figure 27: **Calculation of W^+, W^- charge asymmetry as a function of rapidity, measured through their lepton decays. Ratios relative to calculations with no nuclear effects are also shown. From arXiv:1905.01486 [hep-ex]. See also Albacete *et al.*, NPA for predictions by Ru *et al.*.**

Top Quarks!

First predicted for photoproduction, then in p+Pb collisions and measured by CMS in 3 different channels

$R_{p\mathrm{Pb}}$ for $t\bar{t}$ production at 8 TeV: d'Enterria

Significant differences between EPS09 and EPPS16 – larger effect predicted for EPS09

No uncertainties shown but even at this high scale they would be non-negligible

Not able to measure these distributions yet but at higher energies, as in the FCC, rates would be high enough for the measurements to be feasible

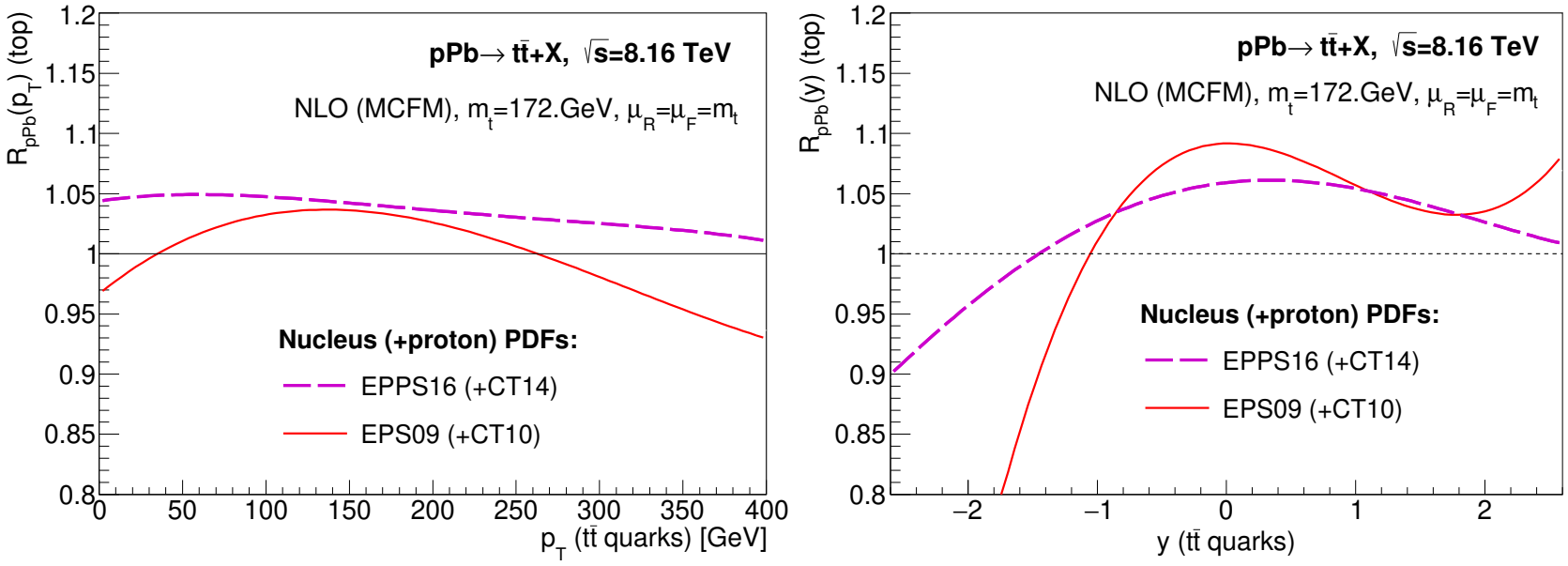

Figure 28: **Nuclear modification factors as a function of transverse momentum (left) and rapidity (right) for $t\bar{t}$ production in the ℓ+jets channel at $\sqrt{s_{NN}} = 8.16$ TeV for the produced top quarks. Predicted by d'Enterria and appearing also in Albacete *et al.*, NPA.**

Top quark cross sections in $p+p$ and p+Pb at 8 TeV

Large uncertainties but first measurement with limited statistics, could be improved, particularly at something like FCC with ions

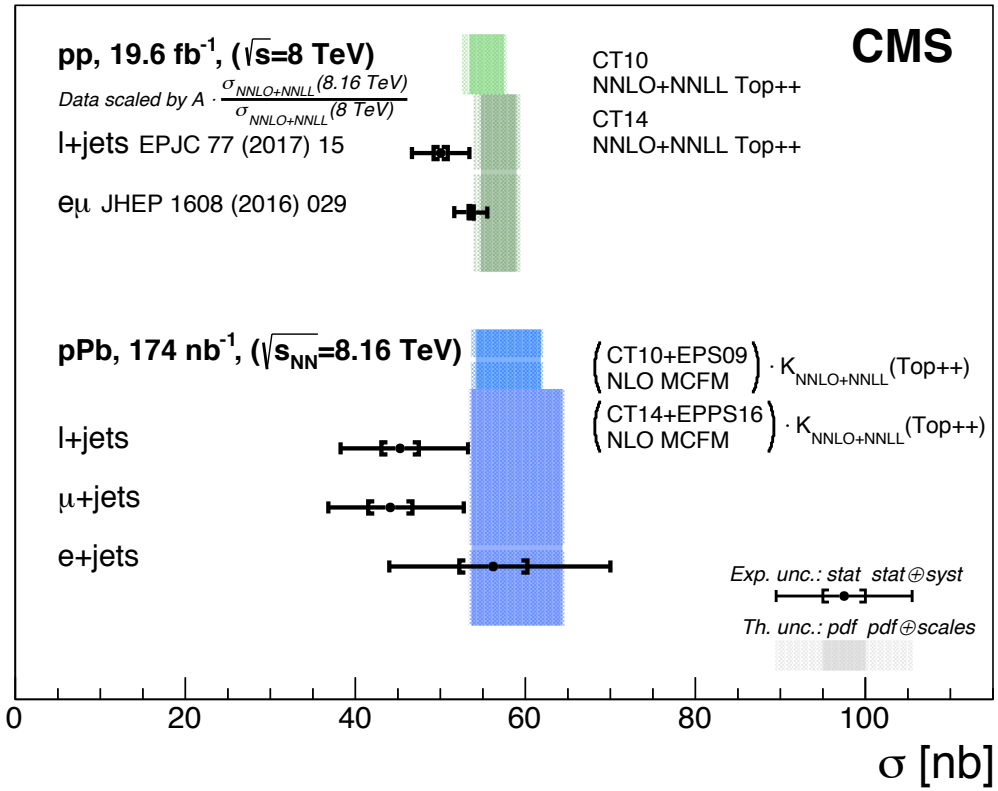

Figure 29: **CMS measurement of $t\bar{t}$ production in different channels in $p+p$ and p+Pb collisions. (PRL 119 (2017) 242001.)**

Summary

- **Uncertainties in quarkonium production likely largest because gluon density in nuclei still unknown, many models exist, even for production in $p + p$ collisions**
- **Progress in nuclear parton densities, LHC data presented here and still to come will bring more improvements**
- **Latest set by Eskola and collaborators is the first to incorporate LHC p+Pb data, finally entering a regime where x can be low and Q^2 is high**
- **Hard probes in $p + A$ collisions at LHC and, at higher x, $e + A$ collisions at the EIC, we can better understand nuclear PDFs and cold nuclear matter in general**
- **$W^{\pm}$ measurements in p+Pb are now mature enough, with sufficient statistics, to clearly distinguish nuclear effects on the parton densities**
- **With measurements of the top quark cross section in p+Pb collisions, we enter a new of perturbative probes of nuclear matter with higher luminosities and more statistics for all hard probes in the future**